Chiral discrimination of amino acids upon binding to achiral anionic polyoxometalates

Bahareh Afsari[1], Vinaya Siby[2], Ruibo Hu[1], Xiaohan Xu[1], Anusree Sundar[2], Nita Sahai[1], Ulrich Kortz[2*], and Tianbo Liu[1*]

[1]School of Polymer Science and Polymer Engineering, The University of Akron, Akron, Ohio 44325, USA

[2]School of Science, Constructor University, Campus Ring 1, 28759 Bremen, Germany

Received: 28 August 2026; **Revised:** 22 November 2026; **Accepted:** 22 November 2026

*Address correspondence to Ulrich Kortz, ukortz@constructor.university; Tianbo Liu, tliu@uakron.edu

Cite This: ***Polyoxometalates*, 2027, *6*, 9140179** https://doi.org/10.26599/POM.2026.9140179

Abstract: The origin of biological homochirality remains a central question in chemistry and early evolution. Here, we show that simple amino acid (AA) enantiomers exhibit chiral discrimination when binding to achiral metal-oxide polyanions ($\{\alpha_2\text{-}P_2W_{17}\}$ and $\{\alpha_2\text{-}As_2W_{17}\}$) in aqueous solution. Using sedimentation velocity analytical ultracentrifugation (SV-AUC), calorimetry, and spectroscopy, we quantify the number of AAs associated with individual polyanions and their binding strengths. We find that certain AAs exhibit enantioselective binding, with one enantiomer binding more strongly than the other. This discrimination is temperature dependent, with D-AAs favored at lower temperatures and L-AAs at higher temperatures. At a given temperature, selectivity occurs within a limited hydrophobicity range. These results reveal a physicochemical pathway by which simple inorganic systems may contribute to prebiotic chiral selection.

Keywords: chiral discrimination, enantioselective binding, polyoxometalates, prebiotic chemistry

Just Accepted

Introduction

This work is dedicated to the memory of Professor Michael T. Pope, whose foundational studies on polyoxometalate chemistry first demonstrated that some metal–oxygen molecular clusters, though regarded as achiral from their structures, can possess an intrinsic chiral character capable of stereoselective interaction with chiral molecules in solution (1). Pope's observation of a Pfeiffer-like optical response in oxidized and reduced octadecamolybdodiphosphate anions anticipated, by several decades, the central premise explored here: that formally achiral polyoxometalates need not be passive with respect to molecular chirality and may instead actively participate in its discrimination and selection. In this work, we build directly on this legacy in showing an interesting phenomenon that the well-defined, achiral Wells–Dawson clusters can enantioselectively discriminate amino acids during binding in aqueous solution. While the observation described here is fascinating, it still lacks a complete scientific explanation. We have the expectation that the early observation from Pope might eventually provide a satisfactory answer in the future.

Homochirality of life on Earth remains a fundamental question in the origin of life (2–9). Chemical evolution is thought to require prior enantiomeric enrichment through a symmetry-breaking event. Although extraterrestrial materials were once considered racemic, small enantiomeric excess (ee) of AAs and sugars has been detected in meteorites (10). Several mechanisms have been proposed to explain such pre-enrichment, including asymmetric UV photodecomposition in space (11) and processes related to the ee of isovaline observed in meteorites, (12) though reported ee values remain below 3%. It is not high enough for the

enantiomeric purity needed for ordered prebiotic self-assembly (13). More recently, enantioselective crystallization of ribo-aminooxazoline on magnetite surfaces under a magnetic field produced ee values of ~60%, (14) while other hypotheses invoke parity-violating forces or spin-polarized particles (15–17).

Miller's classic experiments demonstrated that basic building blocks of life could form in a "primordial soup," but the pathway to complex biomolecules such as proteins and DNA remains unclear (18). Mineral environments, including tidal pools or microscopic cavities in rocks, have been proposed as sites that could promote segregation and organization of biomolecules (19, 20). Supporting this idea, minerals such as calcite at alkaline hydrothermal vents can stabilize AAs long enough for further interactions (21), suggesting that inorganic materials may have contributed to the emergence of homochiral biomolecules. Previous studies have revealed the emergence of chirality in achiral molecules and assemblies (1, 22, 23). Here, we investigate the role of achiral polyoxometalates (POMs) in AA chiral selection, whose well-defined metal–oxygen frameworks enable controlled studies of AA binding and potential enantioselective interactions in solution. (24, 25). Because the POMs serve here as soluble molecular models of metal-oxide mineral surfaces, we use "adsorption" only where we draw this analogy; the interaction measured in solution is a molecular binding (association) of the AAs to the polyanions and is referred to as binding throughout.

Results and Discussion

Chiral Discrimination of AAs During Binding to an Achiral Polyanion $[\alpha_2\text{-}P_2W_{17}O_{61}]^{10-}$

The achiral (C_{2v}) monolacunary Wells–Dawson polyanion $K_{10}[\alpha_2\text{-}P_2W_{17}O_{61}]\cdot 20H_2O$ (**K-1**) (26) was first used for AA binding. CD spectra of a highly diluted solution of **1** (0.125 mg/mL) remained within the noise level of the measurement between 230 and 300 nm (Fig. S3), confirming that free **1** is CD-silent (within ±0.4 mdeg between 300 and 230 nm), as expected from its C_{2v} symmetry. This species derives from the plenary $[\alpha\text{-}P_2W_{18}O_{62}]^{6-}$ polyanion and exists as two monolacunary isomers, $[\alpha_2\text{-}P_2W_{17}O_{61}]^{10-}$ with a cap vacancy and $[\alpha_1\text{-}P_2W_{17}O_{61}]^{10-}$ with a belt vacancy, (27) with the α_2 form being more stable (26, 28, 29). The $[\alpha_2\text{-}P_2W_{17}O_{61}]^{10-}$ ion has idealized C_{2v} symmetry and is therefore achiral, whereas the α_1 isomer is chiral (C_1) (30). **K-1** has been studied in various applications (30, 31).

Just Accepted

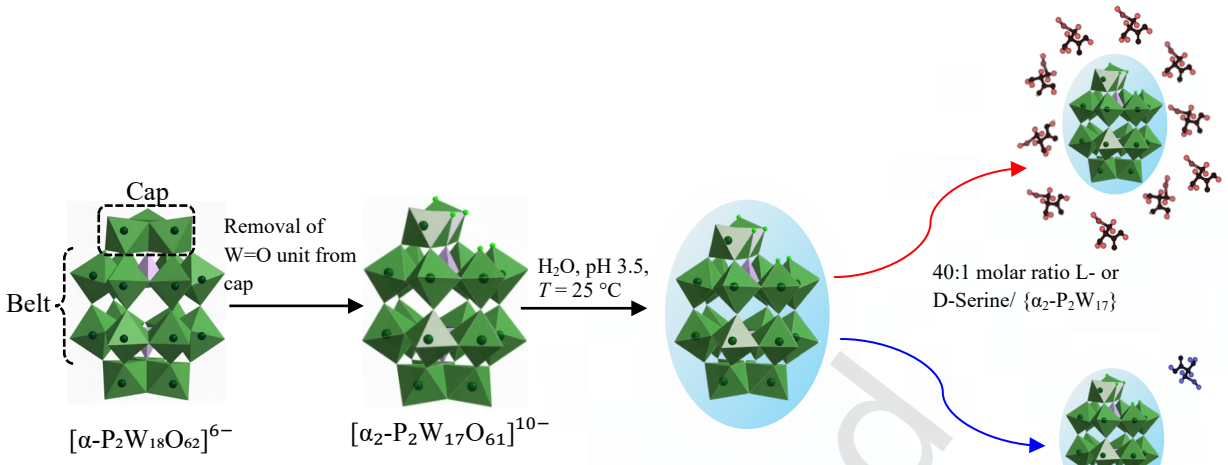

Fig. 1 The monolacunary α2-Dawson $\{\alpha_2\text{-}P_2W_{17}\}$ is formed by removing a W=O group from one of the two caps of $\{\alpha\text{-}P_2W_{18}\}$ polyanion. In water at pH =3.5 and 25 °C, when exposed to both D- and L-Serine, the polyanion demonstrates a strong preference for binding of L-Serine, with minimal binding observed for D-Serine. Color code: WO_6 green octahedra, PO_4 lavender tetrahedra, O neon green spheres.

Isothermal Titration Calorimetry (ITC) experiments were first conducted to investigate the interaction between various essential and non-essential (Table S1 and Fig. S1) L- and D-AAs with **1**, by gradually titrating the AA solution into the solution of **1**. Both solutions are at pH=3.5, and a molar concentration ratio of AA/1 = 40 was used to provide a sufficient excess relative to the ~10 negative charges per polyanion, ensuring near-saturation conditions. AAs are classified into hydrophilic, neutral, and hydrophobic groups according to the K&D hydropathy scale (Table S1) (32). The pH of 3.5 was chosen because 1 is stable under these conditions (29, 37) and because it lies within the range of moderately acidic waters (pH 2–5) found in terrestrial hydrothermal fields, which are widely discussed as plausible settings for prebiotic chemistry (55, 56). K-**1** dissolves completely under these conditions, giving K^+ concentrations of about 10 mM in ITC (1.0 mM **1**) and 0.4 mM in SV-AUC (0.04 mM 1); because the K^+ concentration and ionic strength are identical for the L- and D-enantiomer of each pair, counterions cannot by themselves produce enantioselectivity. At pH=3.5, the neutral and hydrophobic AAs are mostly zwitterion species, whereas the hydrophilic AAs carry a full +1 charge. A typical set of ITC data is shown in Fig. 2, where the thermodynamic parameters and the stoichiometry of the AA–polyanion interaction can be obtained. For example, in Fig. 2, the experiment compares the titration of Serine enantiomers to **1** using 25 droplets (10 µL each), measuring the heat at each step at 25 °C. Data fitting based on independent model reveals the binding strength by association constant parameter (K_a) and enthalpy and entropy changes.

Just Accepted

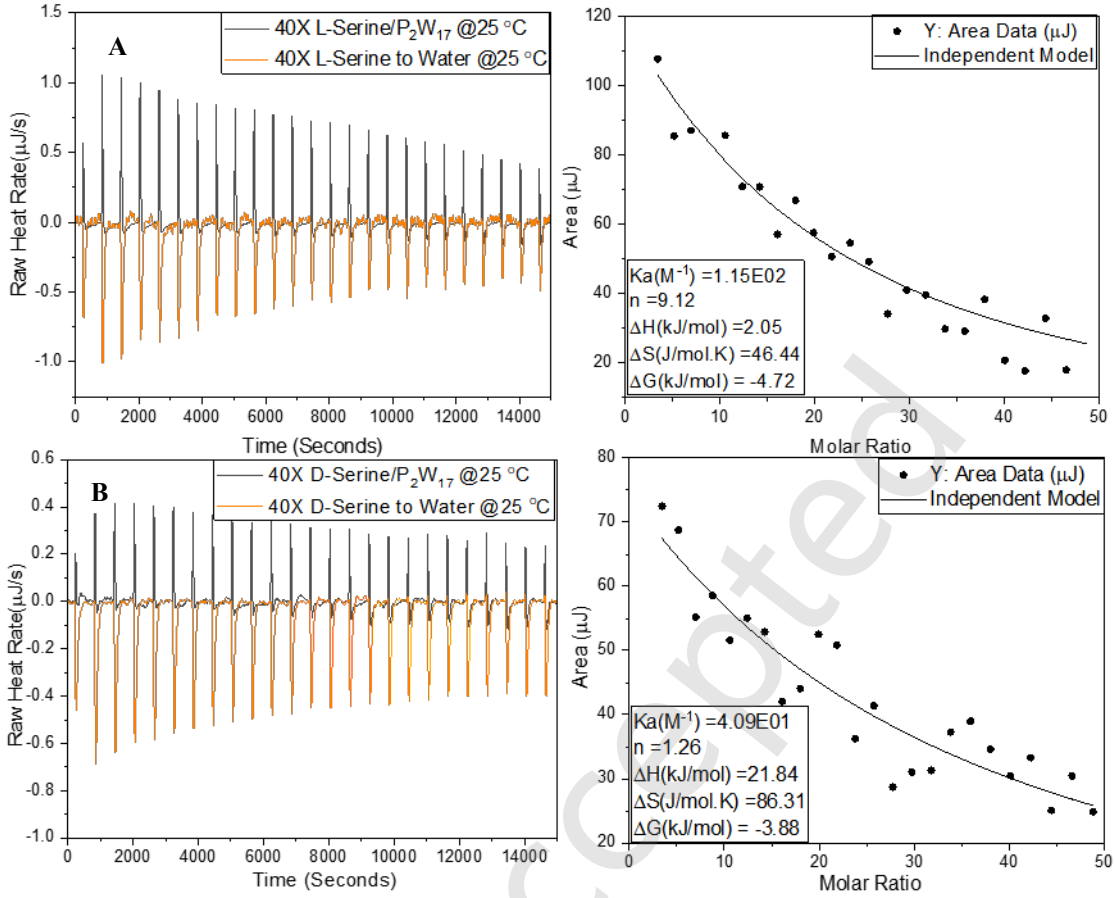

Fig. 2 The ITC experiment involved titrating 25 droplets, each 10 μL, of Serine into a single polyanion solution in acidic water at pH 3.5, maintaining a constant amino acid-to-{α_2-P_2W_{17}} ratio of 40:1. The solid orange line represents the titration of the amino acid into the solvent, while the solid black line indicates the interaction between the amino acid and the polyanion. The data were fitted using an independent binding model for: (A) L-Serine to the polyanion, and (B) D-Serine to the polyanion.

The binding of Serine enantiomers to the surface of **1** is weakly endothermic from the ITC data. Surprisingly, L- and D-Serine show completely different thermodynamic behaviors. The D-Serine/**1** interaction exhibits less favorable enthalpic contribution and is primarily driven by favorable entropy, whereas L-Serine/**1** shows a more pronounced enthalpic contribution to binding. The primary distinction lies in the binding number (n), with nine L-Serine binding to **1** (n = 9.1, $K_a = 1.15 \times 10^2$), while D-Serine/**1** exhibits a significantly lower binding number of 1.3, suggesting that the L-Serine exhibits significant binding, whereas D-Serine shows almost no effective binding onto **1**.

To verify this observation, SV-AUC measurement was performed on the same system. The sedimentation coefficient (s) was obtained by fitting time-dependent radial concentration profiles to the Lamm equation (33). Figure 3A shows the s distribution for a 0.2 g/L (0.04 mmol/L) solution of **1** containing 1.63 mmol/L L- or D-Serine. For pure **1**, s = 3.38 S, with S referring to the unit of sedimentation, Svedberg (Figure 3A), corresponding to an R_h value of 0.91±0.05 nm (34). The presence of L- or D-Serine leads to shifts in s values, indicating their binding to **1**. According to the Svedberg equation (Eq. S5), these changes arise from variations in molecular weight (M) and hydrodynamic radius (R_h) upon AA binding.

Just Accepted

According to Fig. 3A, *s* for D-Serine-**1**=3.64 S and for L-Serine-**1**=3.79 S, a difference beyond experimental error. Moreover, the number of bound AA molecules, determined by the ITC experiments, also contributes to the *M* value. Using Eq. S5 the R_h of **1** after binding L- and D-Serine molecules can be calculated: with L-, $R_h = 0.99 \pm 0.05$ nm and D-, $R_h = 0.87 \pm 0.05$ nm. While the R_h of L-Serine/**1** increased from the value of 1, that of D-Serine/1 (0.87 ± 0.05 nm) lies within experimental uncertainty of the value of bare 1 (0.91 ± 0.05 nm), indicating much weaker binding of D-Serine to 1. Because the L- and D-samples contain the same amino acid concentration, a small increase in *s* from partial screening of the charge of **1** by free amino acid would affect both enantiomers equally. The calculation also assumes that the partial specific volume and f/f_0 do not change on binding; partial dehydration or compaction of the hydration shell upon binding (34) therefore cannot be excluded. Overall, these results confirm that more L-Serine molecules bind to 1, which enlarges the apparent R_h value, thus further confirming that there exists a chiral discrimination for Serine-**1** interaction, even though **1** is considered achiral.

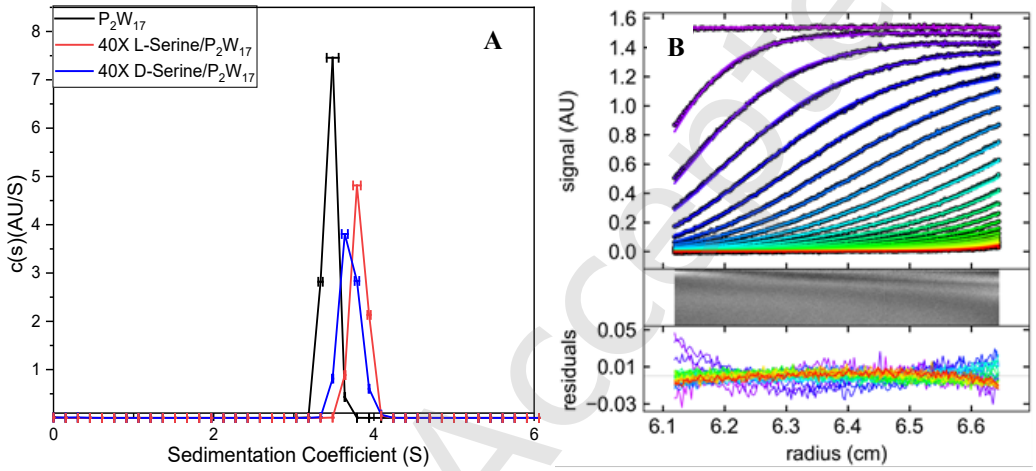

Fig. 3 Sedimentation coefficient distributions of {α2-P_2W_{17}} before and after addition of D- and L-Serine obtained from the c(s) fitting model (35) at 25 °C. (A) Binding of D- and L-Serine to {α2-P_2W_{17}} results in different *s* values, indicating different binding behavior of enantiomers to the polyanion, (B) Sedimentation profiles of D-Serine-{α2-P_2W_{17}}. The top panel represents signal intensity as a function of the radius of the measurement cell at different time points, the middle panel visualizes the sedimentation boundary, and the bottom panel displays residuals, indicating the fit quality of the sedimentation model.

Mapping the general AA binding to 1 at 25 °C

Table S2 summarizes ITC titrations of AAs onto **1** at pH=3.5 (40:1 AA/**1** ratio), showing that other AAs in the neutral region of the K&D scale (Threonine and Tryptophan) also bind more strongly in their L-form than their D-enantiomers at 25 °C, as indicated by greater heat release and higher binding numbers.

L-Threonine bound to **1** with $n = 6.6$, compared to $n = 3.7$ for D-Threonine; both interactions are weakly endothermic with comparable enthalpic contributions, with $\Delta H = 7.48$ and 8.12 kJ/mol, respectively. L-Tryptophan bound with $n = 8.5$, releasing $\Delta H = -0.70$ kJ/mol, whereas D-Tryptophan exhibited negligible binding and no detectable enthalpy change. The other two AAs in this region of the hydropathy scale, Tyrosine and Proline, showed very little net heat release (Table S2), indicating that binding between these AAs and **1** is negligible; therefore, no detectable chiral discrimination was observed due to the lack of effective binding. The weak interaction is

Just Accepted

likely due to the relatively more hydrophilic nature of these two AAs than the others in the "neutral zone" of the K&D hydropathy scale.

The SV-AUC data collected for the same group of AAs (Figs. 5A and B) reveal that those AAs showed distinct thermodynamic behaviors and different *s* values. L- and D-Threonine bound to **1** with s = 3.63 S and 3.79 S, corresponding to R_h = 0.97 and 0.94 nm, respectively, based on the ITC-derived n values. L- and D-Tryptophan exhibited s = 3.48 S and 3.64 S, yielding R_h = 1.09 and 0.84 nm, respectively; in both cases confirming more L-AAs are bound to **1**. The s values obtained from solutions of **1** containing Tyrosine or Proline are identical with that of pure **1** (Fig. 5C, Fig. S4C), further confirming that these two AAs interact with **1** negligibly.

For more hydrophilic AAs (Histidine, Lysine and Arginine), they are fully protonated at pH=3.5 therefore carry more effective charges than the hydrophobic and neutral AAs. ITC data (Table S2) reveal high association constants and negative values of $\Delta G°$ of association, indicating strong binding between them and **1** with binding stoichiometries ~3–4. However, the thermodynamic parameters for each enantiomeric pair are nearly identical, indicating no chiral preference in binding. Similarly, SV-AUC results (Fig. S4D-F) show no difference in the s values between L- and D-enantiomers for this group. These AAs, which contain two or more amine groups, become doubly protonated in acidic aqueous conditions, facilitating strong electrostatic interactions with the negatively charged **1**, which enhances binding affinity but suppresses chiral discrimination. Because both enantiomers of each AA carry the same charge, electrostatic attraction cannot by itself generate enantioselectivity. However, it governs the overall binding strength and thus where in the hydropathy scale discrimination becomes observable; when Coulomb attraction dominates, as for His, Lys and Arg, the small free-energy difference between diastereomeric complexes is masked.

For two hydrophobic AAs tested, Alanine and Methionine, ITC data show that binding involves a small enthalpic penalty, but the interactions are entropy-driven, resulting in negative $\Delta G°$ values for all cases. Despite this, the binding numbers remain low, suggesting that these AAs almost do not interact with **1**. SV-AUC studies show that the s values of their L- and D-enantiomers overlap completely, indicating no enantioselective binding (Figs. S4A and S4B). Overall, we can conclude that at 25 °C the chiral discrimination in AA binding does not exist for both hydrophilic and hydrophobic AAs, likely due to different reasons: for hydrophobic ones, the AA–polyanion interaction is too weak to be effective; for hydrophilic ones, the interaction is very strong so that the delicate difference due to chirality is suppressed. In the middle region, we observed clear preferential binding for L-enantiomers for Serine, Threonine and Tryptophan.

Temperature Effect of Amino Acid Binding

Since the hydrophobicity of AAs shows to be a factor on the observed chiral discrimination when interacting with **1,** the effect of temperature becomes important because AAs exhibit increased effective hydrophobicity at elevated temperatures. ITC experiment performed at 40:1 molar ratio of AA to **1** at 10 °C showed lower association constant (K_a) values than those at 25 °C, indicating weaker interactions between AAs and **1** due to higher AA solubility at lower temperatures. However, despite the low binding affinity, the number of binding sites and other thermodynamic parameters differ between two enantiomers for Alanine and Methionine in the hydrophobic AA group. Within the neutral region, Tryptophan, Threonine, Tyrosine and Proline all show that the D-enantiomers reach the binding number of ~6 to 10 to **1**, whereas the L-enantiomers show minimal to no binding. Progressing into the hydrophilic AA region, the D-enantiomers continue to show higher binding numbers than the L-enantiomers (Table S2).

SV-AUC at 10 °C showed that eight out of ten examined AAs exhibited subtle differences in values of L- or D-binding onto **1**. Fig. 5D–F and Fig. S5 illustrate how these differences were

Just Accepted

observed in three distinct groups of AAs based on their relative hydropathy on the K&D scale and their charge.

Similar experiments performed at 15 °C showed that AA – polyanion binding remains generally weak, yet differences among AAs are still discernible. In all cases exhibiting chiral discrimination, the D-enantiomer remains favored (Table S2).

The intriguing transition from L-favored to D-favored due to temperature prompted us to examine the situation at 20 °C. The observed trend resembled that previously seen at 25 °C, with L-AAs being more favored in the neutral region.

Raising the temperature further to 35 °C (Fig. S6, Table S2) results in no significant difference between L- and D-enantiomer binding of the hydrophobic and neutral AAs onto 1, except for Proline, the most hydrophilic of the neutral AAs. However, notable differences emerge in the hydrophilic region: Histidine and Lysine exhibit comparable binding numbers, but with significantly different binding strengths. For Histidine, the *K*a difference between enantiomers reaches approximately 2,200 M^{-1}, while Lysine and Arginine show *K*a ratios of about 4 and 2, respectively. Across all the AAs displaying distinct thermodynamic behavior, the L-enantiomer consistently shows favored binding to **1**. The chiral discrimination seen for Arginine arises from both greater binding number and stronger affinity for the L-enantiomer, that for Proline from a greater binding number, whereas for Histidine and Lysine, the discrimination is driven solely by differences in binding strength.

Fig. 4 represents the summary of the observations in all three regions at five different temperatures. Overall, chiral discrimination between the enantiomers has been more broadly observed for AAs at low temperatures, where D-enantiomers are favored for binding. At higher temperatures, L-enantiomers become more favored, and at each temperature only a narrow range of AAs demonstrate the chiral discrimination. This range tends to shift towards hydrophilic side with increasing temperature.

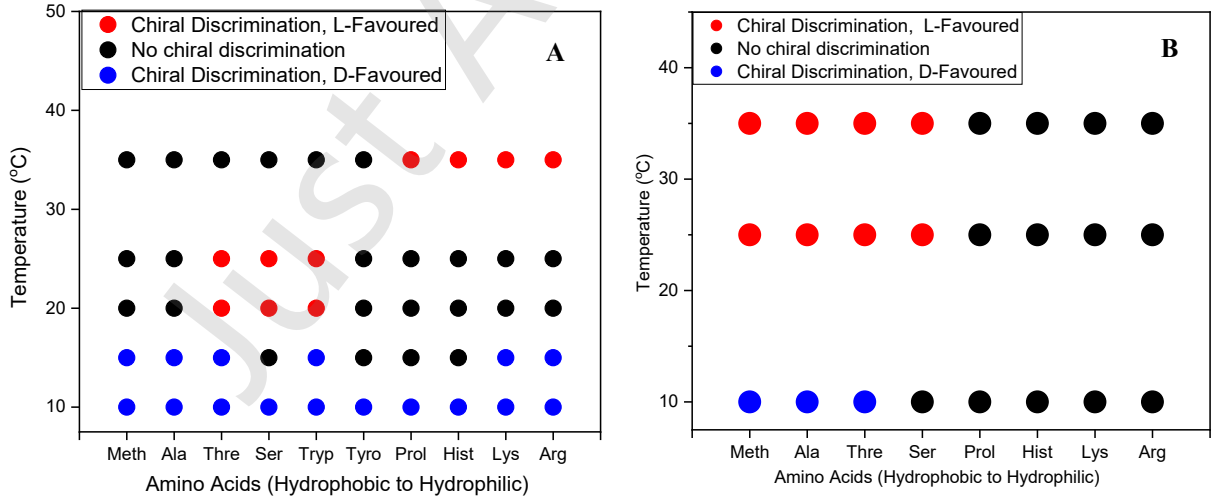

Just Accepted

C

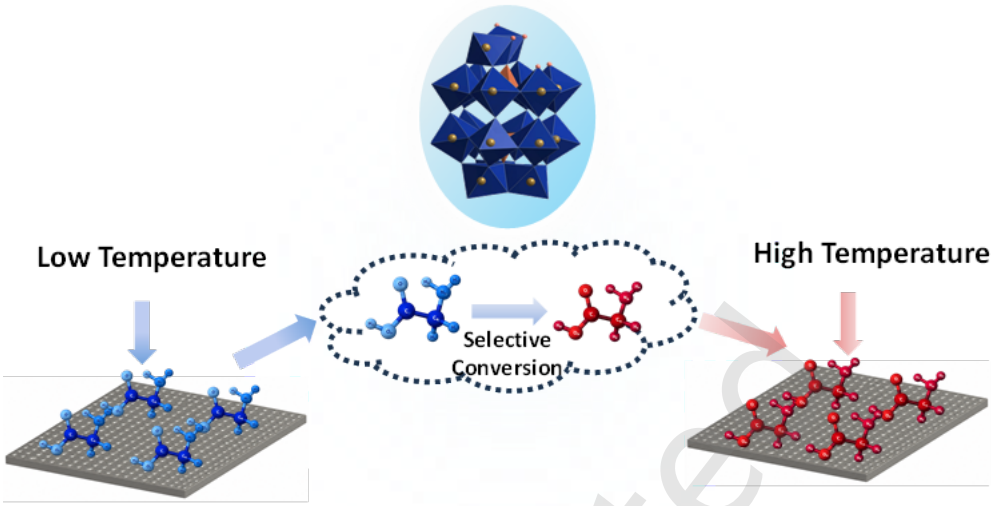

Fig. 4 Chiral discrimination of amino acids (AAs) interacting with (A) {α_2-P_2W_{17}} **1** and (B) {α_2-As_2W_{17}} **2** at different temperatures, determined from ITC and SV-AUC measurements. AAs are arranged according to their K&D hydropathy index, enabling correlation between molecular polarity and enantioselective binding. Distinct, temperature-dependent "discrimination windows" are observed, where preferential binding shifts from D-AAs at lower temperatures to L-AAs at higher temperatures. Enantioselectivity is most pronounced within intermediate hydropathy ranges and diminishes when interactions become either too weak (hydrophobic regime) or too strong (hydrophilic regime). (C) Schematic showing that, for 2, heteroatom substitution (P → As) retains chiral discrimination while shifting the window, with D-AAs favored at low temperature and L-AAs at 25 and 35 °C. Color code: WO_6 dark blue octahedra, AsO_4 orange tetrahedra, O orange spheres. Blue/red molecules refer to the D/L AAs respectively and the light blue oval refers to the hydration shell. A pair is classified as discriminating when ITC (n differing by >30% or K_a by >50%) and SV-AUC ($\Delta s \geq 0.10$ S or $\Delta R_h \geq 0.05$ nm) both show a difference beyond experimental uncertainty.

Increasing temperature enhances hydrophobicity and strengthens AA binding to **1**, shifting the chiral discrimination toward neutral AAs because the hydrophobic AAs would interact with **1** strongly so that the delicate chiral discrimination cannot sustain. As shown in Fig. 4, D-favored discrimination dominates at 10 and 15 °C. With further increasing temperature, the discriminated AAs shift from hydrophobic to neutral and eventually hydrophilic, and from 20 °C L-enantiomers become favored. Circular Dichroism (CD) spectra of hydrophilic AAs mixed with **1** at 35 °C (Fig. 5J–L) show negative and positive Cotton effects for D- and L-enantiomers, respectively, with the D- signal markedly stronger. The D/L optical rotation ratios (insets) deviate from the symmetric value of −1 to −3, indicating freer D-enantiomers in solution and consistent with preferential binding of L-enantiomers to **1**.

Just Accepted

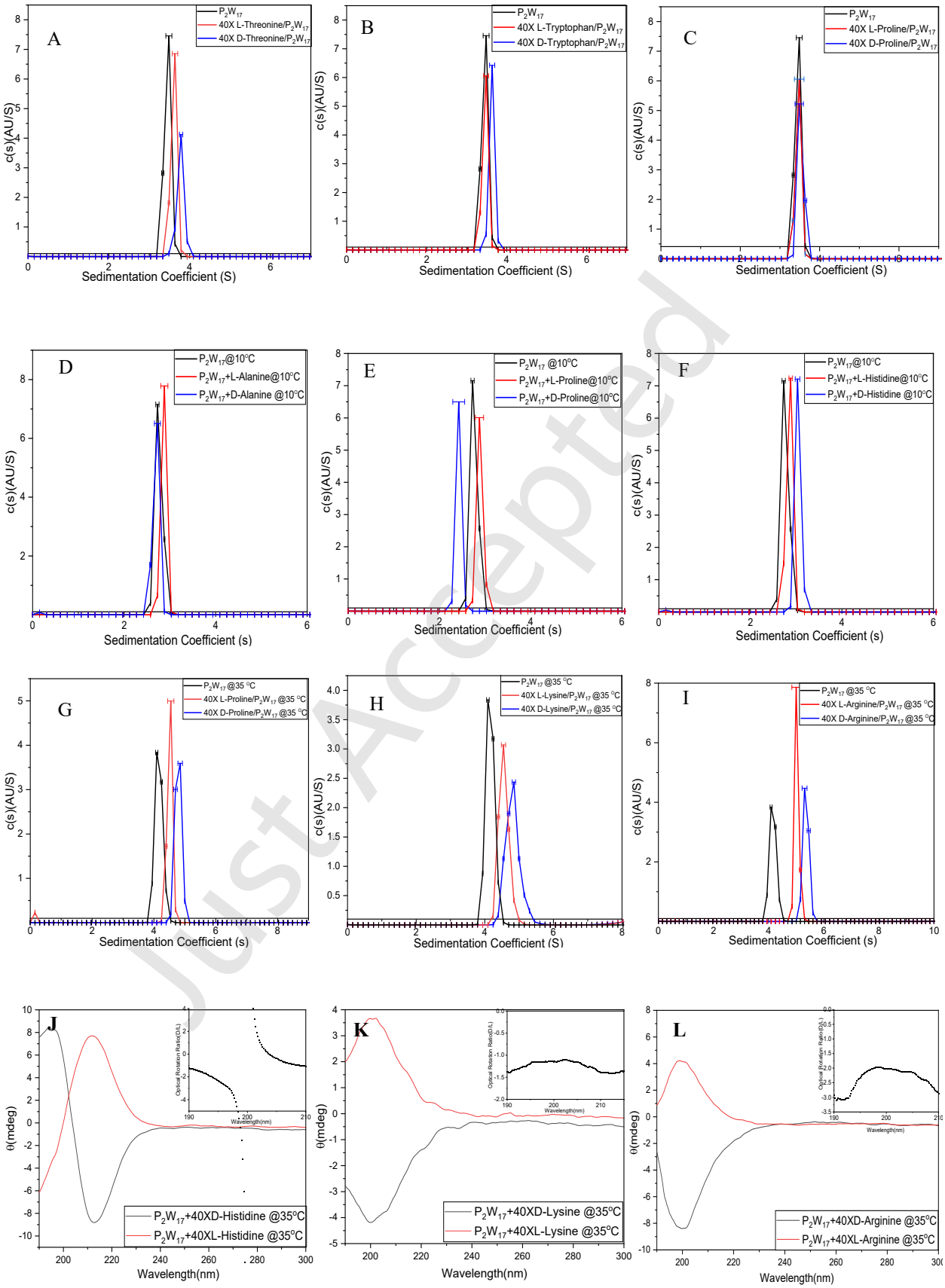

Just Accepted

Fig. 5 Temperature-dependent variations in the s-values of amino acid (AA) enantiomers bound to {α_2-P_2W_{17}} **1**. At 25 °C, these differences become confined to neutral AAs (A) Threonine/**1**, (B) Tryptophan/1, and this difference disappeared in **(**C) Proline/**1**. At 10 °C, pronounced differences are observed for hydrophobic AAs e.g., (D) Alanine/**1**, most neutral AAs e.g., (E) Proline/**1**, and all hydrophilic AAs e.g., (F) Histidine/**1**. At 35 °C, the selectivity boundary shifts toward the hydrophilic region, beginning at the terminal neutral residue (G) Proline/**1** and extending across basic AAs (H) Lysine/**1**, (I) Arginine/**1**. CD spectra of (J) Histidine/**1**, (K) Lysine/**1**, and (L) Arginine/**1** at 35 °C (40:1 AA:**1** molar ratio) reveal strong chiral discrimination, with D-enantiomers displaying enhanced negative Cotton effects relative to the positive Cotton effects of the corresponding L-enantiomers.

Is P_2W_{17} Polyanion Unique?

To determine whether this chiral discrimination is unique to **1** or more general, we examined the mono-lacunary Wells–Dawson analogue $K_{10}[\alpha_2\text{-}As_2W_{17}O_{61}]\cdot 21H_2O$ (**K-2**) (Fig. S11). This polyanion shares the same structural framework as **K-1**, differing only in the central heteroatom, allowing direct evaluation of how heteroatom substitution (P^{5+} vs. As^{5+}) influences electronic and binding properties.

To probe temperature effects, identical experiments with **2** were conducted at 10, 25 and 35 °C (Table S3, Fig. 4B). At 10 °C, hydrophobic amino acids (Alanine and Methionine) show slightly higher K_a values in AA-2 than in AA-1, with D-enantiomers favored in both systems; however, enantioselectivity is more pronounced in AA-1 (Tables S2, S3). With increasing polarity, Threonine shows comparable K_a for L- and D-forms in AA-**2**, whereas in AA-1 the D-enantiomer binds ~60-fold more strongly, with a larger difference in n (5.9 vs 0.2 in AA-1; 5.8 vs 1.3 in AA-**2**). Serine shows negligible binding in AA-**2**, whereas in AA-**1** the two enantiomers show distinct n values (3.8 vs 7.2). For more hydrophilic amino acids, K_a values in AA-2 are similar to or slightly higher than those in AA-1, with no chiral discrimination.

Interestingly, at 25 °C, binding in hydrophobic AA-**1** becomes stronger but loses chiral discrimination, whereas AA-**2** remains weakly bound, preserving observable enantioselectivity. In this regime, polar amino acids behave similarly to 10 °C: *K*a values for AA-**2** are lower than AA-**1**, with retained but weak chiral discrimination – L- favored for Threonine and only marginally for Serine. In the hydrophilic region, binding to AA-**2** is moderate and enantioselectivity disappears.

At 35 °C, in the hydrophobic AAs, a difference between L- and D- persists with L- favored, though the disparity decreases compared to lower temperatures. In the polar region, despite weak binding in AA-**2**, the difference becomes more pronounced, again favoring L- for both Threonine and Serine. Moving further into the hydrophilic region, chiral discrimination by AA-**2** disappears.

Electrochemical studies of Dawson-type heteropolyanions show that **1** has a more positive reduction potential than **2**, indicating it is more easily reduced (36). This difference arises from the higher electronegativity and smaller ionic radius of P^{5+}, which withdraws electron density from the W–O framework and makes **1** more electron-deficient, whereas the As^{5+} center in **2** allows greater electron delocalization and slightly more negative reduction potentials (36). These electronic differences lead to distinct AA interaction profiles, with the more electron-deficient **1** favoring interactions with more polar amino acids, while **2** shows a shift toward less polar, more hydrophobic AAs.

The polyanion $[\beta_2\text{-}SiW_{11}O_{39}]^{8-}$ is inherently chiral and so we decided to also examine the salt $K_8[\beta_2\text{-}SiW_{11}O_{39}]\cdot 14H_2O$ (**K-3**), which exists as a racemic mixture (Fig. S12). Because **3** is unstable at pH values above ~1.5, it was examined under this condition rather than at pH 3.5 used for **1** and **2**. At pH 1.5 and 25°C, **3** did not show any chiral discrimination when binding with Methionine, Serine, and Lysine, representing typical amino acids from different regions of the K&D scale (Fig. S7).

Just Accepted

Similarly, at 10°C and 35 °C, **3** showed no chiral discrimination. This clearly shows that the chiral discrimination reported above is not a very general phenomenon among the metal-oxide polyanions, and so far, we have only observed this with two monolacunary Wells-Dawson polyanions.

Potential Mechanism of AA Chiral Discrimination by Achiral Polyanions

To confirm that the observed chiral discrimination is intrinsic and not caused by chemical instability, the integrity of **1**, the more stable of the two monolacunary isomers (28), was examined at pH 3.5 (28, 37). Because phosphotungstate equilibria can be shifted by added species (58), the stability of **1** was examined both alone and in the presence of L- and D-Serine. As shown in Fig. S8, quantitative ^{31}P NMR spectra of **1** at pH 3.5 show the two resonances of the α_2 isomer (−7.29 and −14.41 ppm at 25 °C) in a 1:1 ratio. The spectra remain unchanged in the presence of 40 equivalents of L- or D-Serine after at least 24 h at 25 and 35 °C, i.e. under the conditions and for the duration of the ITC and SV-AUC experiments: no new signals appear, and the positions and integral ratio of the two resonances are unaffected by the amino acid. Under identical conditions, the signals of $[\alpha_1\text{-}P_2W_{17}O_{61}]^{10-}$ (−8.53 and −12.86 ppm) are clearly separated from those of $[\alpha_2\text{-}P_2W_{17}O_{61}]^{10-}$ (−7.33 and −13.48 ppm) (28), and any α_1 isomer formed from achiral precursors would be racemic and could not produce a net preference for one amino acid enantiomer. The single sedimenting species observed in all SV-AUC runs, including at 10 and 35 °C, further supports the integrity of 1. In the presence of L- or D-Serine, small mirror-image CD signals (1–2 mdeg, 3–6 times the noise level) are observed below 225 nm (Figs. S9, S10). Because this region overlaps the intrinsic CD band of serine, we attribute these signals tentatively to a weak chiral induction of the polyanion by the bound amino acid, reminiscent of the Pfeiffer effect (1). Recent studies have shown that chirality can be induced via hydrogen bonding, for example, when water is confined within cyclic sugar molecules, (22) or when small chiral molecules transfer their handedness to achiral star-shaped block copolymers in solution. (23) Similarly, given that the studied Wells–Dawson polyanions are highly soluble and possess hydration shells (34), chiral induction by the AAs to the polyanions is also likely. This effect is absent in racemic polyanion **3**, which has slightly thinner hydration shell than **1** (34); thus, no chiral discrimination was detected. A particularly intriguing aspect of this study is observed switchable chiral discrimination, where the preference between D- and L-enantiomers changes with temperature. This behavior resembles phenomena reported in brushite crystals, where dynamic nonequilibrium states regulate enantioselective adsorption (38).

The precise molecular origin of this selectivity remains unclear. One possibility is that the bound AAs induce a weak, transient chirality in the polyanions, which exists only while the AAs are bound, consistent with the demonstrated capacity of polyoxometalate macroions to undergo dynamic, counterion-responsive self-assembly and structural reorganization in solution (39–46). Nevertheless, this phenomenon reminds us about the proposed mechanism of homochirality of life – when the basic amino acids were synthesized in the prebiotic ocean, their adsorption onto the rocks and the consequent segregation might be the key step for the chiral selection, leading to the homochirality we see today.

Conclusion

In summary, we demonstrate that two achiral metal-oxide polyanions $\{\alpha_2\text{-}P_2W_{17}\}$ and $\{\alpha_2\text{-}As_2W_{17}\}$ can induce enantioselective **binding of amino acids** in aqueous solution. At a given temperature, they both could induce chiral discrimination for some amino acids within a narrow region of the K&D hydropathy scale, while lower temperatures favor D-amino acids and higher temperatures favor L-amino acids. Raising temperature also shows the tendency of shifting the

Just Accepted

range of discrimination towards the hydrophilic amino acid side. The chiral discrimination disappears when the amino acids – polyanion interaction becomes too strong or negligible. While the exact mechanism of this phenomenon remains unclear, it is speculated that it may arise from a weak, transient chirality induced in the polyanions by the bound chiral amino acids. It is intriguing to relate this observation to the emergence of homochirality in nature, where amino acids have been proposed to undergo enantioselective segregation upon adsorption onto mineral surfaces in prebiotic ocean environments.

Methods

Polyanions 1 ($\{\alpha_2\text{-}P_2W_{17}\}$), 2 ($\{\alpha_2\text{-}As_2W_{17}\}$), and the chiral/racemic control 3 ($\{\beta_2\text{-}SiW_{11}\}$) were synthesized as their potassium salts following published procedures and characterized by FTIR (Fig. S2) and NMR (Supplementary Text). Amino acid–polyanion interactions were characterized by isothermal titration calorimetry (ITC; TA Instruments Nano ITC) at a fixed 40:1 amino acid-to-polyanion molar ratio in acidified water, fitting integrated heats with an independent binding model to obtain association constants (Ka), binding stoichiometry (n), and enthalpy (ΔH). Sedimentation velocity analytical ultracentrifugation (SV-AUC; Beckman Coulter Optima XL-I) was performed in parallel on the same solutions, and sedimentation coefficient distributions were obtained using the c(s) model in SEDFIT. Circular dichroism (CD) spectra were recorded on a Jasco J-1500 spectropolarimeter. All experiments were repeated across a temperature series (10–35 °C) and for both L- and D-enantiomers of each amino acid. Full experimental details, including reagent sources, polyanion synthesis, and instrument parameters, are provided in the Supplementary Text.

References and Notes:

1. J. F. Garvey, M. T. Pope, Chirality of oxidized and reduced octadecamolybdodiphosphate anions. Observation of a Pfeiffer effect. *Inorg. Chem.* **17**, 1115–1118 (1978).
2. U. J. Meierhenrich, Amino acids and the asymmetry of life. *European Review* **21**, 190–199 (2013).
3. R. M. Hazen, T. R. Filley, G. A. Goodfriend, Selective adsorption of L-and D-amino acids on calcite: Implications for biochemical homochirality. *Proceedings of the National Academy of Sciences* **98**, 5487–5490 (2001).
4. R. Breslow, Z.-L. Cheng, On the origin of terrestrial homochirality for nucleosides and amino acids. *Proceedings of the National Academy of Sciences* **106**, 9144–9146 (2009).
5. M. Crisma, *et al.*, Meteoritic C-alpha-Methylated alpha-amino acids and the homochirality of life: Searching for a link. *Angew. Chem. Int. Ed.* **43**, 6695–6699 (2004).
6. M. Gleiser, S. I. Walker, Life's chirality from prebiotic environments. *Int. J. Astrobiol.* **11**, 287–296 (2012).
7. Q. Sallembien, L. Bouteiller, J. Crassous, M. Raynal, Possible chemical and physical scenarios towards biological homochirality. *Chem. Soc. Rev.* **51**, 3436–3476 (2022).
8. W. A. Bonner, Chirality and life. *Origins of Life and Evolution of the Biosphere* **25**, 175–190 (1995).
9. D. G. Blackmond, The origin of biological homochirality. *Cold Spring Harb. Perspect. Biol.* **2**, a002147 (2010).
10. P. Dalai, H. Kaddour, N. Sahai, Incubating life: prebiotic sources of organics for the origin of life. *Elements* **12**, 401–406 (2016).
11. U. J. Meierhenrich, *et al.*, Asymmetric vacuum UV photolysis of the amino acid leucine in the solid state. *Angew. Chem. Int. Ed.* **44**, 5630–5634 (2005).
12. J. Bocková, N. C. Jones, J. Topin, S. V. Hoffmann, C. Meinert, Uncovering the chiral bias of meteoritic isovaline through asymmetric photochemistry. *Nat. Commun.* **14**, 3381 (2023).
13. M. Liu, L. Zhang, T. Wang, Supramolecular chirality in self-assembled systems. *Chem. Rev.* **115**, 7304–7397 (2015).
14. S. F. Ozturk, Z. Liu, J. D. Sutherland, D. D. Sasselov, Origin of biological homochirality by crystallization of an RNA precursor on a magnetic surface. *Sci. Adv.* **9**, eadg8274 (2023).
15. N. A. Hawbaker, D. G. Blackmond, Energy threshold for chiral symmetry breaking in molecular self-replication. *Nat. Chem.* **11**, 957–962 (2019).
16. P. Cintas, C. Viedma, On the physical basis of asymmetry and homochirality. *Chirality* **24**, 894–908 (2012).
17. J. Takahashi, K. Kobayashi, Origin of terrestrial bioorganic homochirality and symmetry breaking in the universe. *Symmetry 11*, 919 (2019).
18. S. L. Miller, A production of amino acids under possible primitive earth conditions. Science 117, 528–529 (1953).

Just Accepted

19. R. Fasel, M. Parschau, K.-H. Ernst, Amplification of chirality in two-dimensional enantiomorphous lattices. *Nature* **439**, 449–452 (2006).
20. I. Weissbuch, L. Addadi, M. Lahav, L. Leiserowitz, Molecular recognition at crystal interfaces. Science 253, 637–645 (1991).
21. R. M. Hazen, D. A. Sverjensky, Mineral surfaces, geochemical complexities, and the origins of life. *Cold Spring Harb. Perspect. Biol.* **2**, a002162 (2010).
22. L. Zhang, *et al.*, Interfacial Self-Assembly of Sugars at Nanoscale Membranes Leads to Micron-Scale, Spectroscopically Ice-Like Chiral Suprastructures of Water. *J. Am. Chem. Soc.* **147**, 33413–33423 (2025).
23. M. Kim, *et al.*, Hierarchical chiral supramolecular assemblies with strong and invertible chiroptical properties. Science 389, eadu0296 (2025).
24. M. T. Pope, U. Kortz, Polyoxometalates update based on the original article by Michael T. Pope. *Encyclopedia of Inorganic and Bioinorganic Chemistry. Weinheim, Germany: John Wiley & Sons, Ltd* (2012).
25. P. Yin, D. Li, T. Liu, Solution behaviors and self-assembly of polyoxometalates as models of macroions and amphiphilic polyoxometalate–organic hybrids as novel surfactants. *Chem. Soc. Rev.* **41**, 7368–7383 (2012).
26. L.-L. Liu, *et al.*, Structural overview and evolution paths of lacunary polyoxometalates. *Coord. Chem. Rev.* **506**, 215687 (2024).
27. B. Hasenknopf, *et al.*, Chirality in polyoxometalate chemistry. *Eur. J. Inorg. Chem.* **2008**, 5001–5013 (2008).
28. R. Contant, M. Richet, Y. W. Lu, B. Keita, L. Nadjo, Isomerically Pure α1-Monosubstituted Tungstodiphosphates: Synthesis, Characterization and Stability in Aqueous Solutions. *Eur. J. Inorg. Chem.* **2002**, 2587–2593 (2002).
29. R. Contant. Potassium octadecatungstodiphosphates (V) and related lacunary compounds. *Inorganic syntheses* **27**, 104–111 (1990).
30. L. E. Briand, G. T. Baronetti, H. J. Thomas, The state of the art on Wells–Dawson heteropoly-compounds: A review of their properties and applications. *Appl. Catal. A Gen.* **256**, 37–50 (2003).
31. Q.-H. Luo, *et al.*, Coordination of rare-earth elements in complexes with monovacant Wells− Dawson polyoxoanions. *Inorg. Chem.* **40**, 1894–1901 (2001).
32. J. Kyte, R. F. Doolittle, A simple method for displaying the hydropathic character of a protein. *J. Mol. Biol.* **157**, 105–132 (1982).
33. O. Lamm, A New Method for determining the Concentration Gradient in the Ultra-Centrifuge Cell. *Nature* **132**, 820–821 (1933).
34. X. Xu, *et al.*, Direct Determination of Hydration Shell Thickness of Molecular Clusters. *Inorg. Chem. 65, 101–108 (2026).*
35. P. Schuck, *Sedimentation velocity analytical ultracentrifugation: discrete species and size-distributions of macromolecules and particles* (CRC Press, 2016).
36. B. Keita, I. M. Mbomekalle, L. Nadjo, R. Contant, Compared Behaviours of Dawson-Type Tungstodiarsenates and-diphosphates. *Eur. J. Inorg. Chem.* **2002**, 473–479 (2002).
37. R. Lampl, J. Breibeck, N. I. Gumerova, M. S. Galanski, A. Rompel, Wells–Dawson phosphotungstates as mushroom tyrosinase inhibitors: a speciation study. *Sci. Rep.* **11**, 19354 (2021).
38. W. Jiang, *et al.*, Switchable chiral selection of aspartic acids by dynamic states of brushite. *J. Am. Chem. Soc.* **139**, 8562–8569 (2017).
39. J. Zhang, D. Li, G. Liu, K. J. Glover, T. Liu, Lag periods during the self-assembly of {Mo72Fe30} macroions: connection to the virus capsid formation process. *J. Am. Chem. Soc.* **131**, 15152–15159 (2009).
40. T. Liu, *et al.*, Self-recognition among different polyprotic macroions during assembly processes in dilute solution. *Science* **331**, 1590–1592 (2011).
41. T. Liu, Hydrophilic macroionic solutions: what happens when soluble ions reach the size of nanometer scale? *Langmuir* **26**, 9202–9213 (2010).
42. J. M. Pigga, M. L. Kistler, C.-Y. Shew, M. R. Antonio, T. Liu, Counterion Distribution around Hydrophilic Molecular Macroanions: The Source of the Attractive Force in Self-Assembly. *Angew. Chem.* **121**, 6660–6664 (2009).
43. J. M. Pigga, J. A. Teprovich Jr, R. A. Flowers, M. R. Antonio, T. Liu, Selective monovalent cation association and exchange around keplerate polyoxometalate macroanions in dilute aqueous solutions. *Langmuir* **26**, 9449–9456 (2010).
44. H. Li, *et al.*, Isotope and Hydrogen-Bond Effects on the Self-Assembly of Macroions in Dilute Solution. *Chem. Eur. J.* **25**, 16288–16293 (2019).

Just Accepted

45. H. Li, *et al.*, Tuning the Intercage Distance in Charge-Regulated Blackberry-Type Assemblies through Host–Guest Chemistry. *Chem. Eur. J.* **25**, 5803–5808 (2019).
46. H. Li, J. Luo, T. Liu, Modification of the solution behavior of Pd12L24 metal–organic nanocages via PEGylation. *Chem. Eur. J.* **22**, 17949–17952 (2016).
47. I. M. Mbomekalle, *et al.*, Rationalization and improvement of the syntheses of two octadecatungstoarsenates: the novel α-K7 [H4AsW18O62]· 18H2O and the well known symmetrical α-K6 [$As_2W_{18}O_{62}$]· 14H_2O. *Inorganica Chim. Acta* **342**, 219–228 (2003).
48. R. Li, *et al.*, Analytical ultracentrifugation for studying molecular cluster solutions. *Polyoxometalates* **5**, 9140132 (2026).
49. A. Velazquez-Campoy, S. A. Leavitt, E. Freire, "Characterization of protein-protein interactions by isothermal titration calorimetry" in *Protein-Protein Interactions: Methods and Applications*, (Springer, 2015), pp. 183–204.
50. T. Svedberg, Mass and size of protein molecules. *Nature* **123**, 871 (1929).
51. T. Svedberg, L. M. Carpenter, D. C. Carpenter, The molecular weight of Casein. I. *J. Am. Chem. Soc.* **52**, 241–252 (1930).
52. T. Svedberg, B. Sjögren, The molecular weights of amandin and of excelsin. *J. Am. Chem. Soc.* **52**, 279–287 (1930).
53. H. Li, *et al.*, Isolation of the (6, 5) single-wall carbon nanotube enantiomers by surfactant-assisted aqueous two-phase extraction. *Carbon 204*, 475–483 (2023).
54. C. R. Graham, R. G. Finke, The classic Wells–Dawson polyoxometalate, K6[α-P2W18O62]·14H2O. Answering an 88 year-old question: What is its preferred, optimum synthesis? Inorg. Chem. 47, 3679–3686 (2008).
55. B. Damer, D. Deamer, The hot spring hypothesis for an origin of life. Astrobiology 20, 429–452 (2020).
56. V. N. Kompanichenko, Exploring the Kamchatka geothermal region in the context of life's beginning. Life 9, 41 (2019).
57. A. Tézé, G. Hervé, α-, β-, and γ-Dodecatungstosilicic acids: isomers and related lacunary compounds. Inorg. Synth. 27, 85–96 (1990).
58. R. I. Maksimovskaya, Hydrolysis of heteropoly acid $H_3PW_{12}O_{40}$ by ^{31}P NMR. Russ. J. Inorg. Chem. 43, 1825–1837 (1998).

Acknowledgments: T.L. acknowledges support from the National Science Foundation (CBET2309886) and the University of Akron. U.K. thanks the German Research Council (DFG) and Constructor University (formerly Jacobs University) for research support.

Supplementary Materials:
Supplementary Text
Figs. S1 to S12
Tables S1 to S3

Funding:
National Science Foundation (CBET2309886)
German Research Council (DFG)
National Science Foundation (EAR 2144770)
Canadian Institute of Fundamental Advanced Research Earth 4D CF-0376 - CP24-054 and CF-0381 - CP24-062

Author contributions:
T.L. and B.A. conceived the study. B.A. performed the AUC and ITC experiments and conducted data analysis. R.H. and N.S. performed and analyzed the CD experiments. X.X. contributed to data analysis. V.S. and A.S. synthesized the POM samples and provided IR characterization. U.K. contributed POM expertise, including selection of POMs, understanding of their solution

Just Accepted

properties, and interpretation of experimental data. B.A. wrote the manuscript. All authors discussed the results and approved the final version of the manuscript.

Competing interests:
The authors declare no competing financial interest.

Data availability: All data supporting the findings of this study (ITC thermograms and fitted parameters, SV-AUC sedimentation coefficient distributions, CD spectra, and NMR spectra) are available from the corresponding author upon reasonable request.

Code availability: This study did not employ custom code. Data fitting was performed using commercially available software (SEDFIT for SV-AUC; NanoAnalyze for ITC), as described in the Methods.

Just Accepted

Electronic Supplementary Material

Chiral discrimination of amino acids upon binding to achiral anionic polyoxometalates

Bahareh Afsari[1], Vinaya Siby[2], Ruibo Hu[1], Xiaohan Xu[1], Anusree Sundar[2], Nita Sahai[1], Ulrich Kortz[2,†,*], and Tianbo Liu[1*]

[1]School of Polymer Science and Polymer Engineering, The University of Akron, Akron, Ohio 44325, USA

[2]School of Science, Constructor University, Campus Ring 1, 28759 Bremen, Germany

[†]Deceased

*Address correspondence to Ulrich Kortz, ukortz@constructor.university; Tianbo Liu, tliu@uakron.edu

Supporting information to https://doi.org/10.26599/POM.2026.9140179

The PDF file includes:

Supplementary Text
Figs. S1 to S12
Tables S1 to S3

Just Accepted

Supplementary Text
Materials and Methods:

Chemicals were obtained from commercial suppliers and used without further purification. Hydrochloric acid (HCl, M_W = 36.46, Concentration = 36.5-38.0% w/w) was purchased from Fisher Scientific. Water used was purified using the Milli-Q DirectQ3 water purification system.

To prepare acidic water, the pH of Milli-Q water was adjusted using HCl. All stock and diluted solutions were prepared using this acidified water. After preparation, the pH of the final samples was measured to confirm it remained at the desired value; if not, it was adjusted accordingly. For ITC experiments, the stock solution was diluted to 1.0 mmol/L, and for AUC experiments, the concentration of polyanion samples was 0.04 mmol/L. The solvents and solutions were filtered through Millipore MILLEX-LG 0.22 μm PTFE filters to remove any dust.

Polyoxometalate Synthesis

The hydrated potassium salts of Wells-Dawson polyanions $K_6[\alpha\text{-}P_2W_{18}O_{62}]\cdot 14H_2O$ (K-P_2W_{18}) (29) $K_6[\alpha\text{-}As_2W_{18}O_{62}]\cdot 14H_2O$ (K-As_2W_{18}) (47) and the hydrated potassium salts of the monolacunary derivatives $K_{10}[\alpha_2\text{-}P_2W_{17}O_{61}]\cdot 20H_2O$ (K-P_2W_{17}) (29), and $K_{10}[\alpha_2\text{-}As_2W_{17}O_{61}]\cdot 21H_2O$ (K-As_2W_{17}) (29) and $K_8[\beta_2\text{-}SiW_{11}O_{39}]\cdot 14H_2O$ (57) were all synthesized according to the published procedures and characterized by IR (Fig. S2) and NMR spectroscopy. All other chemicals were purchased from Sigma Aldrich and used without further purification.

Synthesis of $K_{10}[\alpha_2\text{-}P_2W_{17}O_{61}]\cdot 20H_2O$

A sample of 40 g (8.25 mmol) of K-P_2W_{18} is dissolved in 100 mL distilled water and a solution of 10 g (0.1 mol) of $KHCO_3$ in 100 mL water is added on stirring. After 1 h, the white precipitate is filtered, dried under suction and redissolved in 250 mL of hot water (95 °C). The solution is then cooled to obtain snow-like crystals of K-P_2W_{17} in 3-4 hours which is then filtered and dried under suction.

Synthesis of $K_{10}[\alpha_2\text{-}As_2W_{17}O_{61}]\cdot 21H_2O$ (K-As_2W_{17})

To a solution of 11.85 g K-As_2W_{18} dissolved in 36 mL H_2O, 36 mL of 1 M $KHCO_3$ was added and stirred at room temperature for 40 minutes. The white precipitate formed was then filtered by suction and redissolved in 50 mL hot water and then allowed to cool. A white crystalline precipitate that was slowly formed was suction-filtered and air-dried.

Synthesis of $K_8[\beta_2\text{-}SiW_{11}O_{39}]\cdot 14H_2O$

Sodium tungstate (18.2 g) is dissolved in 30 mL water. To this solution, 16.5 mL 4 M HCl is added slowly with vigorous stirring.
Another solution prepared by dissolving sodium metasilicate (1.1 g) in 10 mL water is added into the first solution. The pH of the solution is adjusted between 5 and 6 with 4 M HCl and maintained at that pH over a period of 100 min with continuous stirring. KCl (9 g) is then added to this solution and stirred for another 15 min. The white precipitate formed is filtered and redissolved in 85 mL water. Any insoluble material is filtered off, and the salt is precipitated again by addition of 8 g KCl. The precipitate is filtered and washed with 2 M KCl solution and air dried.

Just Accepted

This compound was characterized by FTIR (KBr pellet, cm^{-1}: 988, 945, 875, 855, 805, 730, 610(sh), 530, 460 (sh), 395 (sh), 360, and 325).

Analytical Ultracentrifugation (AUC)

Prior to AUC measurements, all solutions were filtered through a hydrophilic 0.22 μm PTFE membrane. SV experiments were performed on a Beckman Coulter Optima XL-I analytical ultracentrifuge equipped with a four-hole An-60Ti rotor and 12 mm double-sector centerpieces. Samples were equilibrated in the AUC cell for 3 h before each run. Radial calibration and routine performance checks were conducted to ensure measurement accuracy. Data were analyzed using the *c*(s) model in SEDFIT (35). For non-spherical polyanions, the frictional ratio (f/f_0) was obtained through *c*(s) model fitting in SEDFIT (35)**.**

The partial specific volume ($\bar{v}$) of the polyanion solutions was determined by measuring the densities of a series of solutions prepared at different concentrations. Solution densities were obtained using a Portable Density/Specific Gravity Meter (DA-130N, KYOTO Electronics) according to the literature (34). From this, $\bar{v}_{\text{polyanion}}$ was calculated using the equation $\bar{v} = \frac{1-slope}{\rho_s}$. The resulting $\bar{v}$ values were subsequently used as input parameters in SEDFIT for data fitting. For hydrodynamic radius (R_h) calculations using Eq. S5, the intrinsic partial specific volume of the polyanions ($\bar{v}_{\text{polyanion}}$) is required. Because the solid materials used for solution preparation contain counterions and crystallization water, the nominal solution concentrations were corrected to represent only the mass of the polyanion. These corrections were based on the known chemical formulas of the polyanions. Under the highly diluted conditions of the AUC experiments, crystallization water and counterions are assumed to fully dissociate into the bulk solvent (34, 48). For the amino acid–polyanion complexes, R_h was calculated from Eq. S5 with *M* increased by the mass of n bound amino acid molecules (n from ITC), while the partial specific volume and f/f_0 were held at the values of the bare polyanion. Further SEDFIT fitting (35) parameters are listed in the table below.

POM	*s* (S) at 25℃	f/f_0	$\bar{v}_{\text{polyanion}}$	R_h at 25℃
$\{\alpha_2\text{-}P_2W_{17}\}$	3.38±0.05	1.20±0.10	0.11±0.03	0.91±0.05 nm
$\{\alpha_2\text{-}As_2W_{17}\}$	4.84±0.05	1.30±0.10	0.10±0.03	0.65±0.05 nm
$\{\beta_2\text{-}SiW_{11}\}$	2.68±0.05	1.00	0.05±0.01*	0.85±0.02 nm†

Error bars: SD among three independent tests.
*, † Data from literature (34)

^{31}P NMR Spectroscopy

^{31}P NMR spectra were recorded on a Varian NMRS 500 spectrometer (202 MHz for ^{31}P) equipped with a 5 mm dual broad-band probe and on a Bruker 400 MHz spectrometer (162 MHz for ^{31}P), using inverse-gated ^{1}H decoupling. Solutions of K-1 (15 mg/mL) alone or with 40 equivalents of L- or D-Serine (the amino acid/polyanion ratio used in SV-AUC) were prepared in D_2O at pH 3.5 and kept for at least 24 h before measurement; all ITC and SV-AUC experiments were completed within 24 h of sample preparation. Spectra were recorded at 25 °C with relaxation delays of 5, 30, 60 and 100 s, and at 35 °C with a relaxation delay of 100 s. Chemical shifts are referenced on the unified scale (Ξ = 40.480742%). Because the −7.3 ppm phosphorus relaxes slowly ($T_1 \approx 35$ s), equal areas of the two signals are obtained only with long relaxation delays (54); at 100 s the −7.3/−14.4 ppm integral ratio is 0.88–0.94 in all samples. Under identical conditions, [α_1-

Just Accepted

$P_2W_{17}O_{61}]^{10-}$ resonates at −8.53 and −12.86 ppm and $[\alpha_2$-$P_2W_{17}O_{61}]^{10-}$ at −7.33 and −13.48 ppm (28). These experiments were used to examine the stability of $K_{10}[\alpha_2$-$P_2W_{17}O_{61}]\cdot 20H_2O$ in the presence of L- and D-Serine under the conditions (pH, amino acid/polyanion ratio, temperature and time) of the ITC and SV-AUC measurements (58); the polyanion concentration was higher than in SV-AUC (0.2 g/L), at which quantitative ^{31}P spectra are not feasible.

Circular Dichroism (CD) Spectroscopy

CD spectra were recorded using a Jasco J-1500 spectropolarimeter (Jasco, Easton, MD) with a 1 mm pathlength quartz cuvette. Solutions containing the polyanion $K_{10}[\alpha_2$-$P_2W_{17}O_{61}]\cdot 20H_2O$ and amino acids were prepared in acidified water pH=3.5. Spectra were collected over the range of 190–300 nm with a data pitch of 0.2 nm, a bandwidth of 2 nm, a response time of 4 s, and a scan rate of 50 nm min^{-1}. Measurements were performed at 25 °C and 35 °C. Each spectrum represents the average of three accumulations. Background subtraction and spectral smoothing were performed using Spectra Manager software (Jasco), applying a moving-average method with a convolution width of 5. Spectra were corrected with a water blank recorded under identical conditions. The scan-to-scan noise of the polyanion solution was 0.12–0.18 mdeg between 230 and 300 nm ($3\sigma \approx \pm 0.36$ mdeg); below ~225 nm the absorbance exceeds 1.5, and data in this region are shaded in all CD figures and not interpreted quantitatively.

Isothermal Titration Calorimetry (ITC)

ITC experiments were performed using a TA Instruments Nano ITC calorimeter. The instrument was equipped with a 1.0 mL sample cell and an identical reference cell enclosed within an adiabatic shield in a vacuum-tight chamber. In a typical experiment, 1.0 mL of the polyanion solution in acidified water was placed in the sample cell, while the reference cell contained 1.0 mL of acidified water with the same pH. The amino acid solution was loaded into a 250 µL syringe and titrated into the sample cell in 10 µL increments. Control experiments were carried out by titrating the same concentration of amino acid into acidified water to subtract the background heat of dilution. Thermodynamic and binding parameters were obtained by nonlinear fitting of the integrated heat data using the independent binding model, based on the known concentrations of polyanions and amino acids and the heat released upon each injection. Data analysis was performed using NanoAnalyze software (TA Instruments). Details of the fitting model have been described elsewhere (49). The polyanion concentration was 1.0 mM in ITC and 0.04 mM (0.2 g/L) in SV-AUC; since **K-1** dissolves completely, these correspond to K^+ concentrations of about 10 mM and 0.4 mM, respectively, which are identical for the L- and D-enantiomer of each amino acid.

Fourier Transform Infrared (FTIR) Spectroscopy

The infrared (FT-IR) spectra of the samples in the solid state were recorded using KBr discs on a Nicolet Avatar 370 spectrophotometer (400–4000 cm^{-1}) with 32 scans and 4 cm^{-1} resolution.

Theoretical Analysis of Analytical Ultracentrifugation (AUC) Data

The ability to accurately characterize biomacromolecules using Analytical Ultracentrifugation (AUC) sedimentation equilibrium (SE) (50, 51) and sedimentation velocity (SV) (50–52) through key physicochemical parameters such as molar mass, sedimentation, diffusion, and frictional coefficients, as well as shape, has historically been transformative. The fundamental equation governing ultracentrifugation experiments is the Lamm equation (33), as shown in equation Eq. S1. This equation describes the local concentration variations, *c*, of the sample in the ultra-centrifugal field over time, *t*, due to diffusion and sedimentation (represented by *D* and *s*, respectively):

$$\frac{\partial c}{\partial t} = \frac{1}{r}\frac{\partial}{\partial r}\left(rD\frac{\partial c}{\partial r} - s\omega^2 r^2 c\right) \qquad \text{Eq. S1}$$

Just Accepted

where r is the radial position, and ω is the rotor angular velocity.

Hydrodynamic Description of Sedimentation

Previous studies have demonstrated that AUC can probe chiral discrimination through differences in sedimentation coefficients during chiral adsorption processes (53). The sedimentation velocity (SV) measurements were performed on polyanion solutions in the presence and absence of amino acids. The buoyant molar mass M_b is given by:

$$M_b = M_{\text{polyanion}}(1 - \bar{v}\rho_s) \quad \text{Eq. S2}$$

where $M_{\text{polyanion}}$ and $\bar{v}$(cm³/g) are the molar mass and the partial specific volume of the polyanion, respectively, and ρ_s is the solvent density. Balancing the buoyant force with the frictional force f experienced by the particle, the sedimentation coefficient s can be expressed as:

$$s = \frac{M_b}{N_A f} \quad \text{Eq. S3}$$

where N_A is Avogadro's number and f is the frictional coefficient.
For a spherical particle, the frictional coefficient is given by Stokes' law:

$$f_0 = 6\pi\eta R_h \quad \text{Eq. S4}$$

where η is the solvent viscosity and R_h is the hydrodynamic radius. For non-spherical particles such as monolacunary Wells–Dawson polyanions, deviations from spherical geometry are accounted for using the frictional ratio f/f_0, where $f > f_0$.
Substituting into Eq. S3, the sedimentation coefficient can be written as:

$$s = \frac{M_{\text{polyanion}}(1-\bar{v}\rho_s)}{N_A\, 6\pi\eta R_h} \cdot \frac{f_0}{f} \quad \text{Eq. S5}$$

Just Accepted

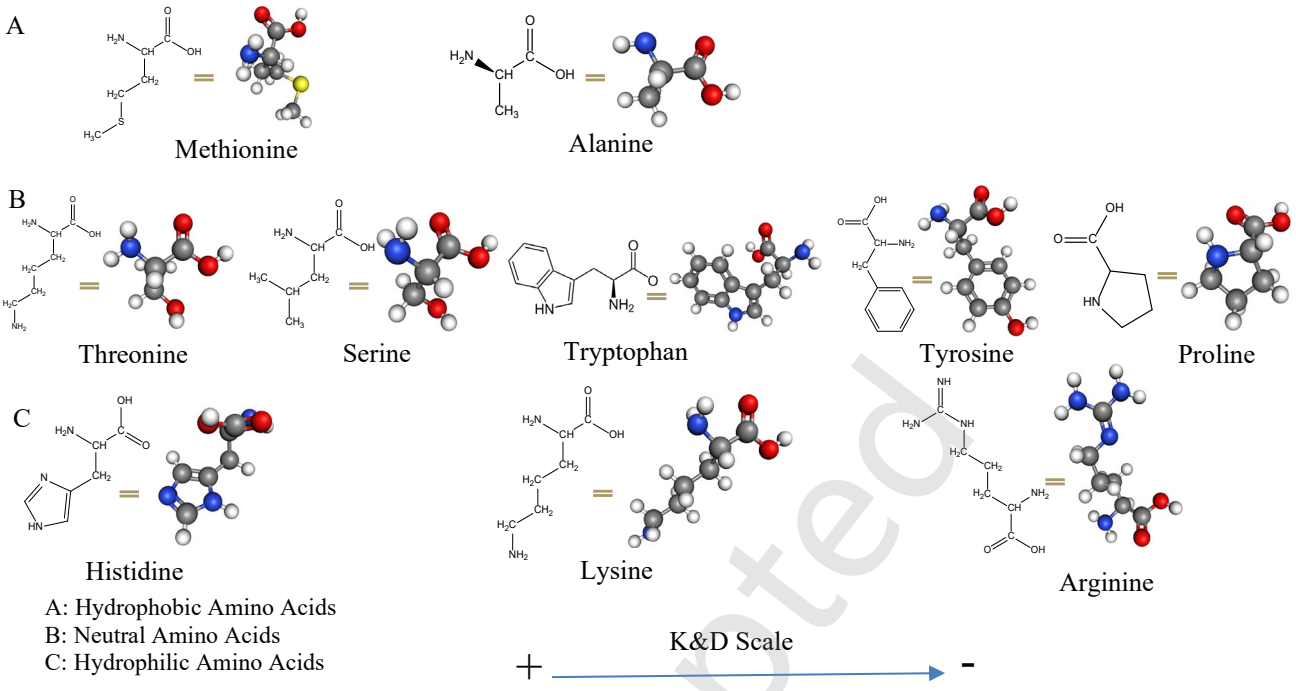

Fig. S1.
Molecular structures of essential and non-essential amino acids, grouped by K&D parameters. Color code: N (blue), O (red), C (grey), H (white), S (yellow).

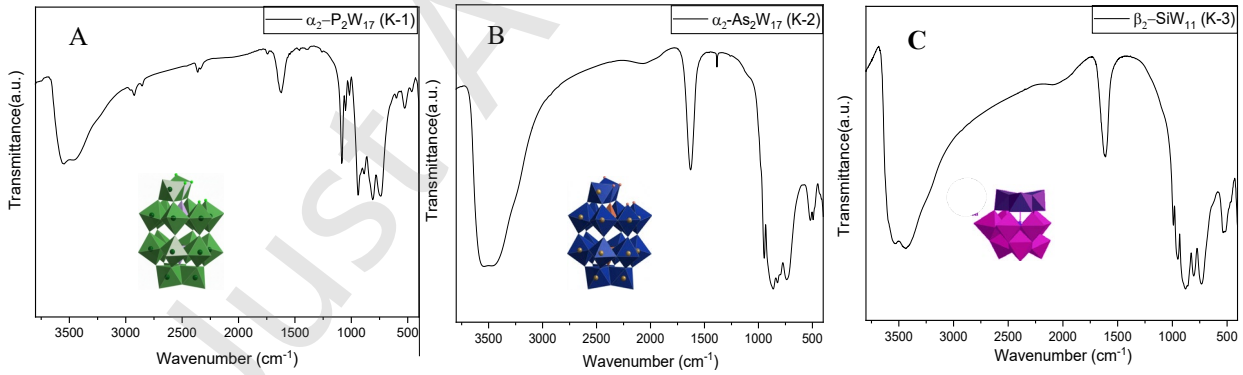

Fig. S2.
FT-IR spectra of the synthesized polyoxometalates**:** (A) $K_{10}[\alpha_2\text{-}P_2W_{17}O_{61}]\cdot 20H_2O$, (B) $K_{10}[\alpha_2\text{-}As_2W_{17}O_{61}]\cdot 21H_2O$, and (C) $K_8[\beta_2\text{-}SiW_{11}O_{39}]\cdot 14H_2O$. The spectra display the characteristic vibrational bands of the tungsten–oxygen framework, including terminal W–O_t and bridging W–O–W stretching modes, confirming the integrity of the polyoxometalate structures.

Just Accepted

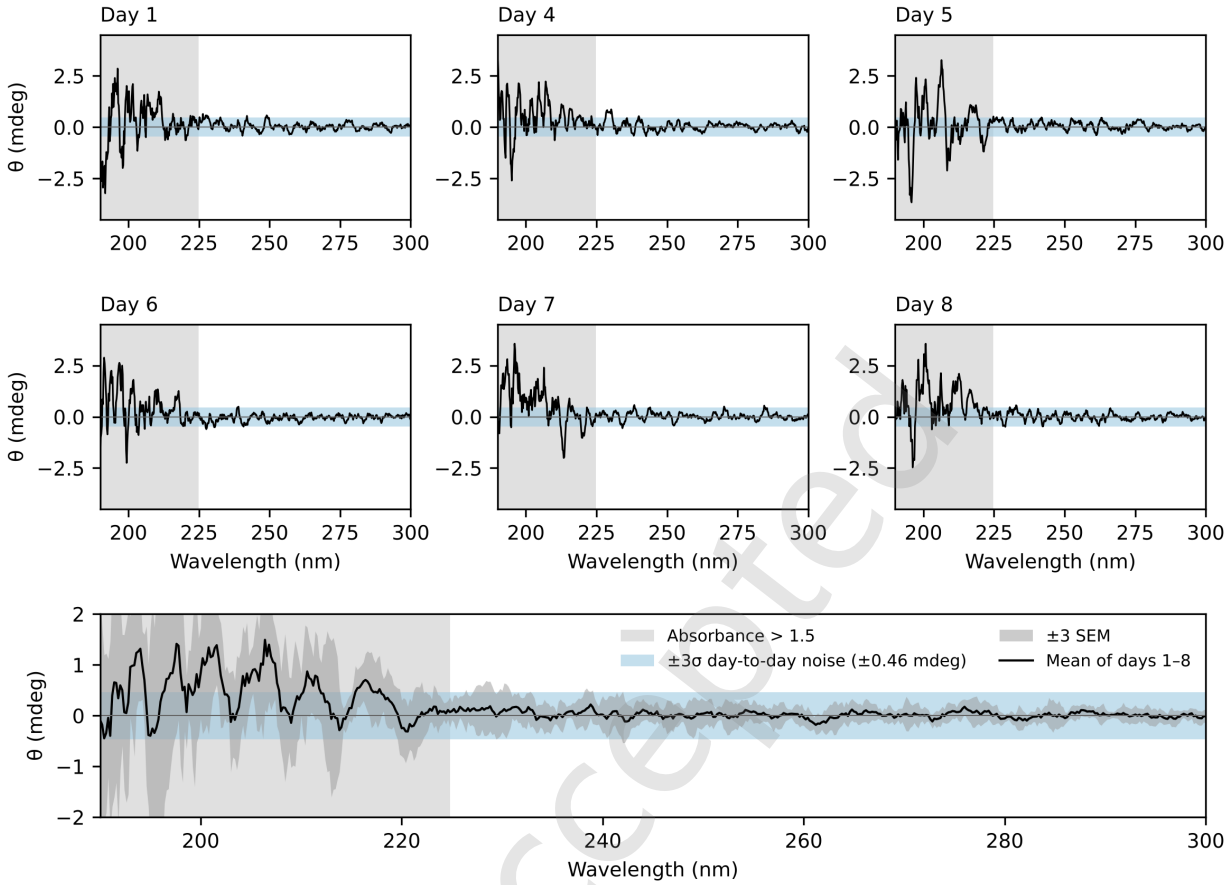

Fig. S3
CD spectrum of 1 (pH 3.5, 25 °C, 1 mm path; mean of three scans, water-blank corrected). Blue band: ±3σ noise; shaded region: absorbance > 1.5.

Just Accepted

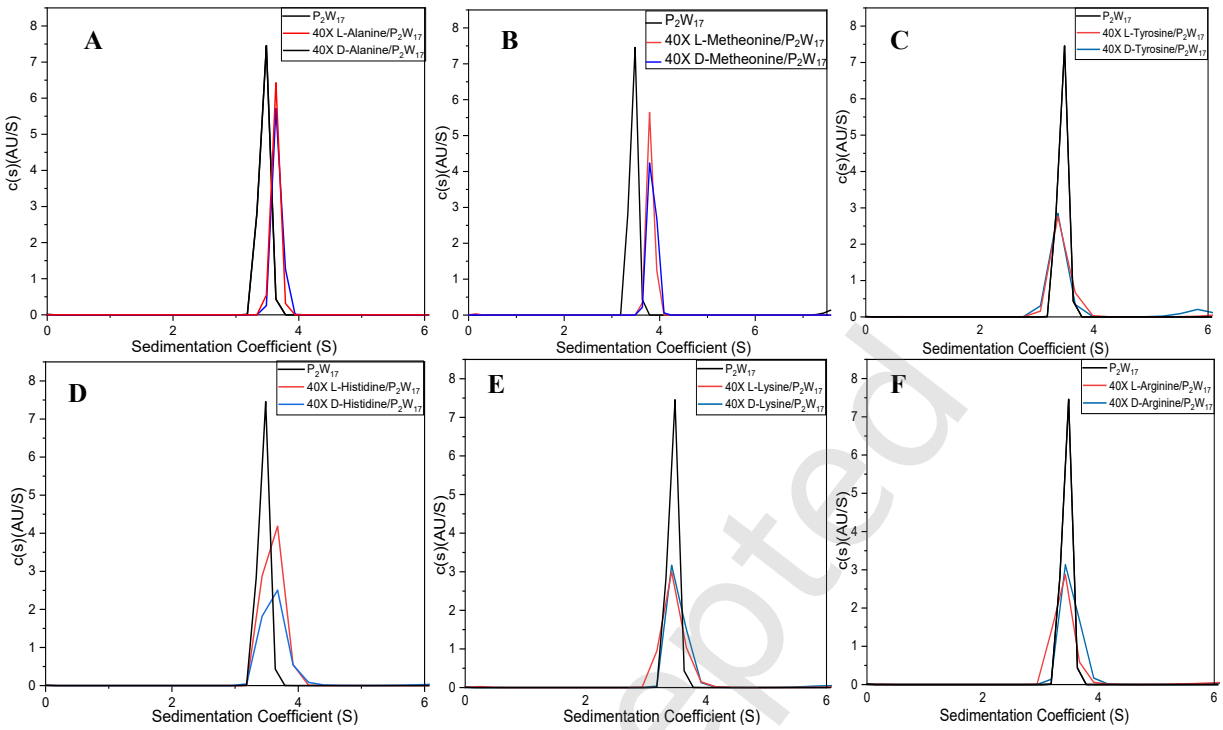

Fig. S4.

SV-AUC analysis of amino acid– $\{\alpha_2\text{-}P_2W_{17}\}$ interactions at a 40:1 molar ratio and 25 °C: (A) D- and L-Alanine, (B) D- and L-Methionine, (C) D- and L-Tyrosine, (D) D- and L-Histidine, (E) D- and L-Lysine, and (F) D- and L-Arginine binding to the surface of $\{\alpha_2\text{-}P_2W_{17}\}$. At 25 °C, moving toward more hydrophobic or highly hydrophilic amino acids eliminates the chiral discrimination by $\{\alpha_2\text{-}P_2W_{17}\}$.

Just Accepted

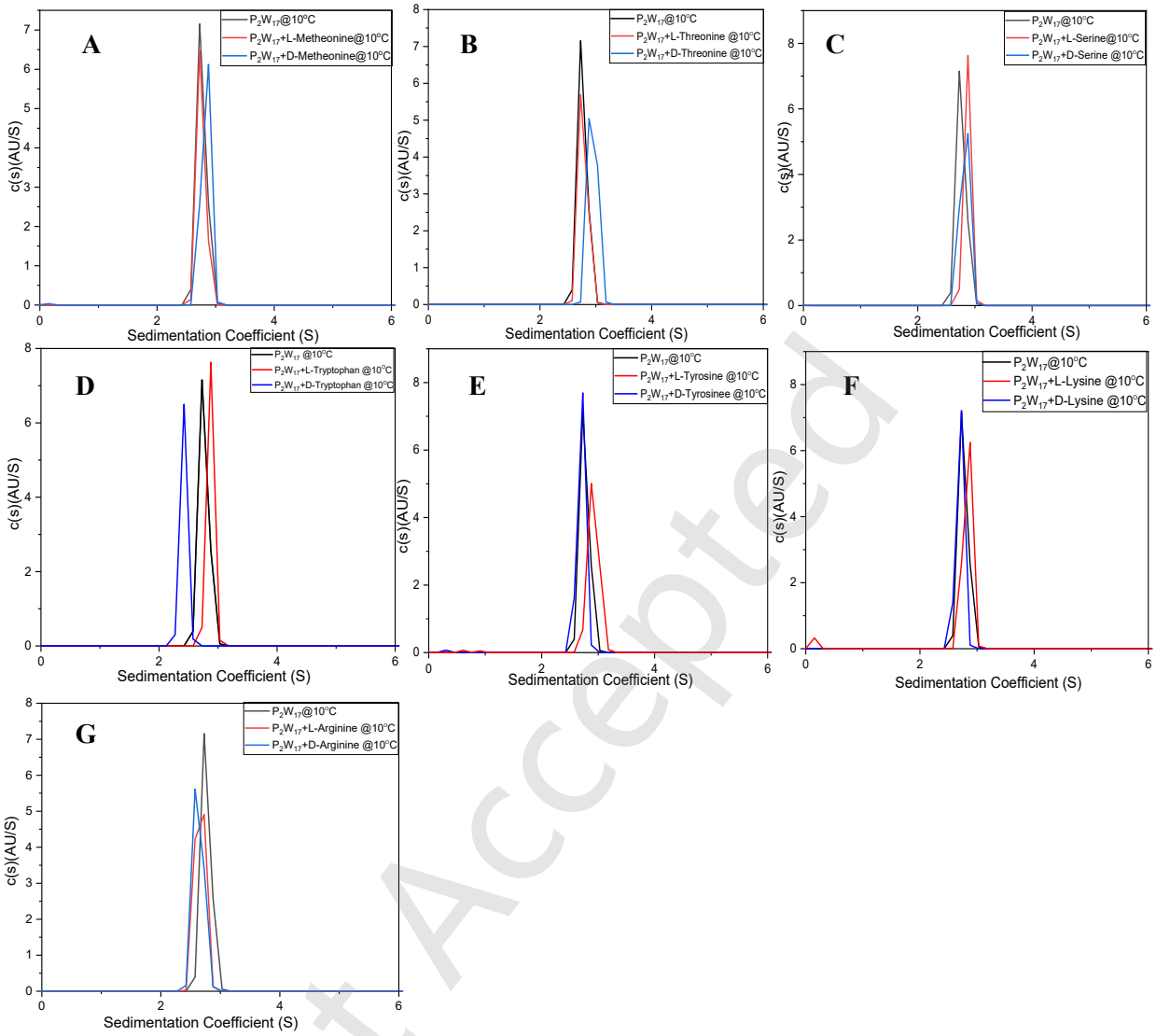

Fig. S5.

SV-AUC analysis of amino acid–{α_2-P_2W_{17}} interactions at a 40:1 molar ratio and 10 °C: (A) impact of D- and L-Methionine, (B) D- and L-Threonine, (C) D- and L-Serine, (D) D- and L-Tryptophan, (E) D- and L-Tyrosine, (F) D- and L-Lysine, and (G) D- and L-Arginine binding to the surface of {α_2-P_2W_{17}}. As shown, six out of the seven amino acid pairs exhibit distinct binding behavior to {α_2-P_2W_{17}} at 10 °C.

Just Accepted

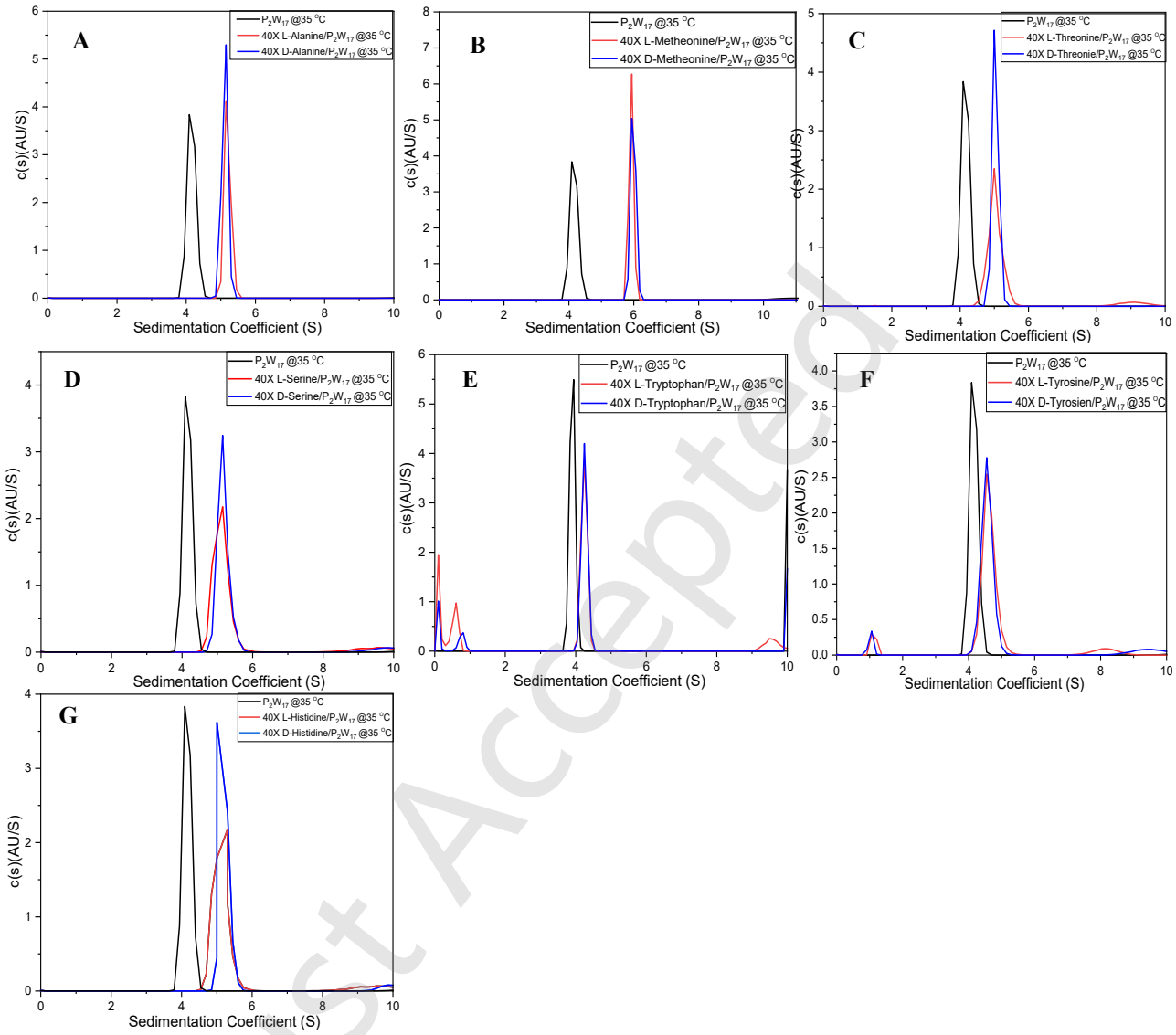

Fig. S6

SV-AUC analysis of amino acid–{α2-P_2W_{17}} interactions at a 40:1 molar ratio and 35 °C: (A) D- and L-Alanine, (B) D- and L-Methionine, (C) D- and L-Threonine, (D) D- and L-Serine, (E) D- and L-Tryptophan, (F) D- and L-Tyrosine, and (G) D- and L-Histidine binding to {α2-P_2W_{17}}. As illustrated, raising the temperature to 35 °C shifts the chiral discrimination effect more prominently toward the hydrophilic amino acids.

Just Accepted

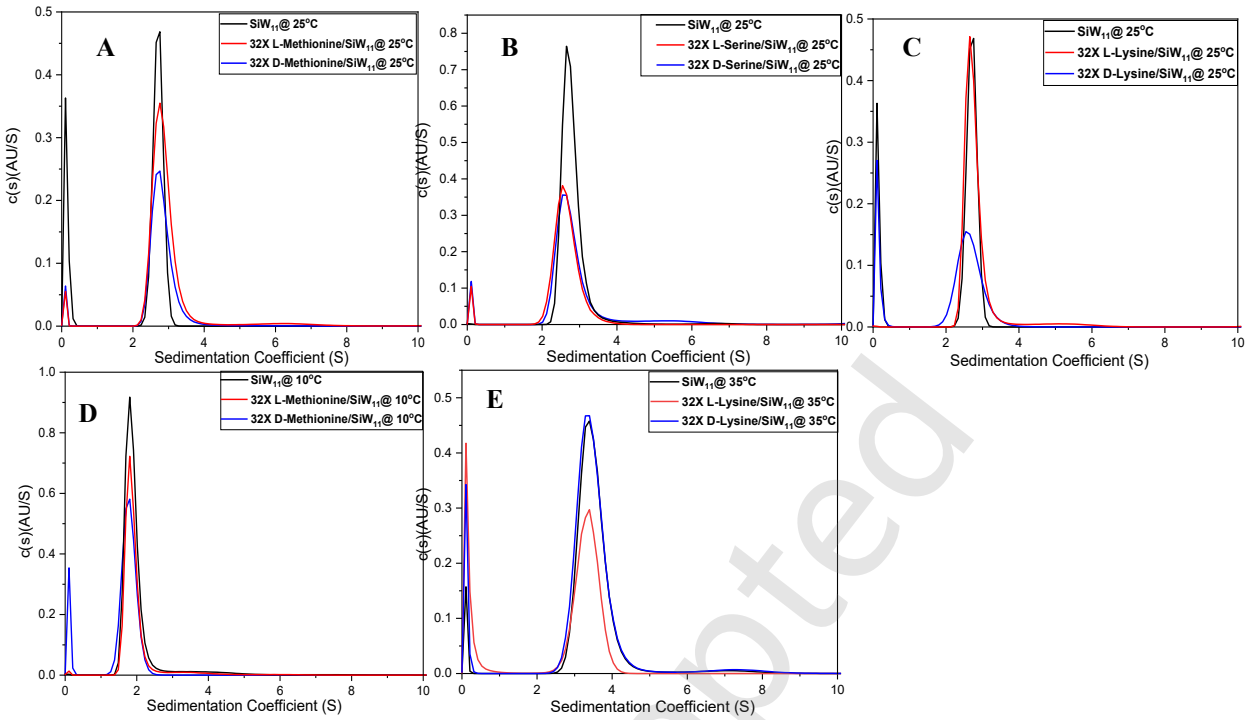

Fig. S7

Chiral discrimination analysis of {β2-SiW_{11}} with (A) Methionine, (B) Serine, and (C) Lysine—three amino acids representing different points on the K&D hydropathy scale at 25 °C. All experiments were conducted in H_2O at pH 1.5 and 25 °C, using a fixed amino acid-to-{β2-SiW_{11}} molar ratio of 32:1. No enantiomeric binding differences were observed under these conditions. (D) Lowering the temperature to 10 °C, previously effective for enhancing chiral selectivity with polyanion {α2-P_2W_{17}}, did not induce any detectable chiral discrimination in this system. (E) Lysine, which previously demonstrated chiral discrimination with {α2-P_2W_{17}} at 35 °C, did not display any such selectivity when tested with {β2-SiW_{11}}.

Just Accepted

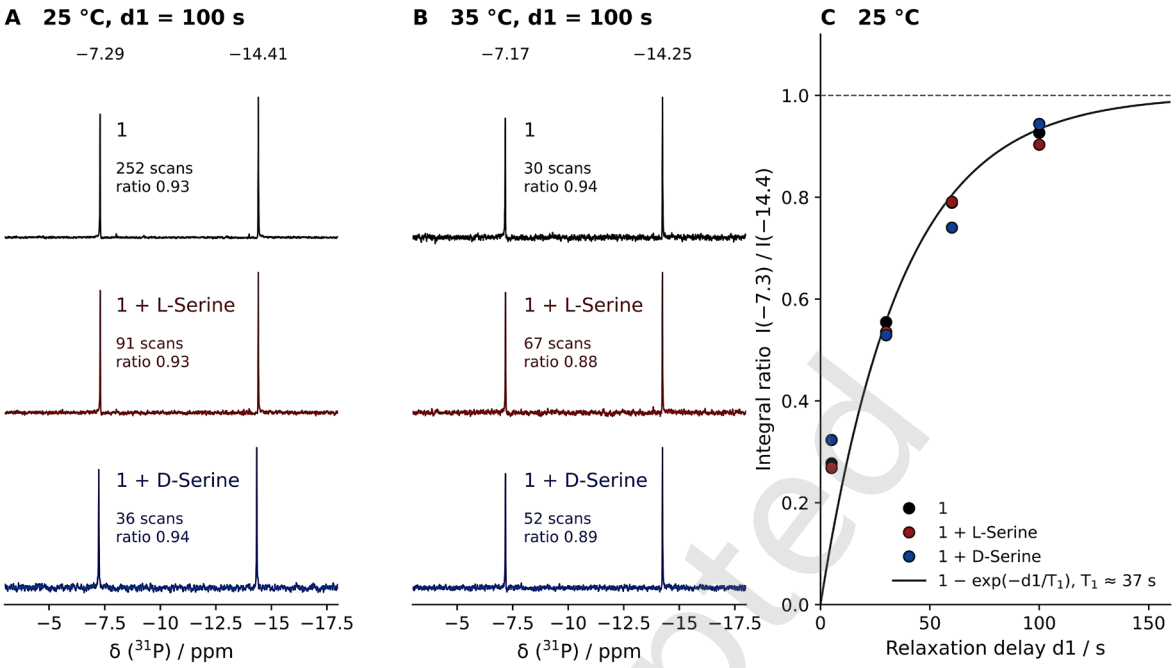

Fig. S8

^{31}P NMR spectra of K-1 (15 mg/mL) alone and with 40 equivalents of L- or D-Serine (pH 3.5, D_2O, ≥24 h after preparation) at (A) 25 °C and (B) 35 °C, recorded with a relaxation delay of 100 s. The two resonances of $[\alpha_2\text{-}P_2W_{17}O_{61}]^{10-}$ are unchanged by L- or D-Serine. (C) Integral ratio of the −7.3 and −14.4 ppm resonances as a function of the relaxation delay at 25 °C; the line is a fit to $1 - \exp(-d1/T_1)$ for a 1:1 ratio ($T_1 \approx 37$ s).

Just Accepted

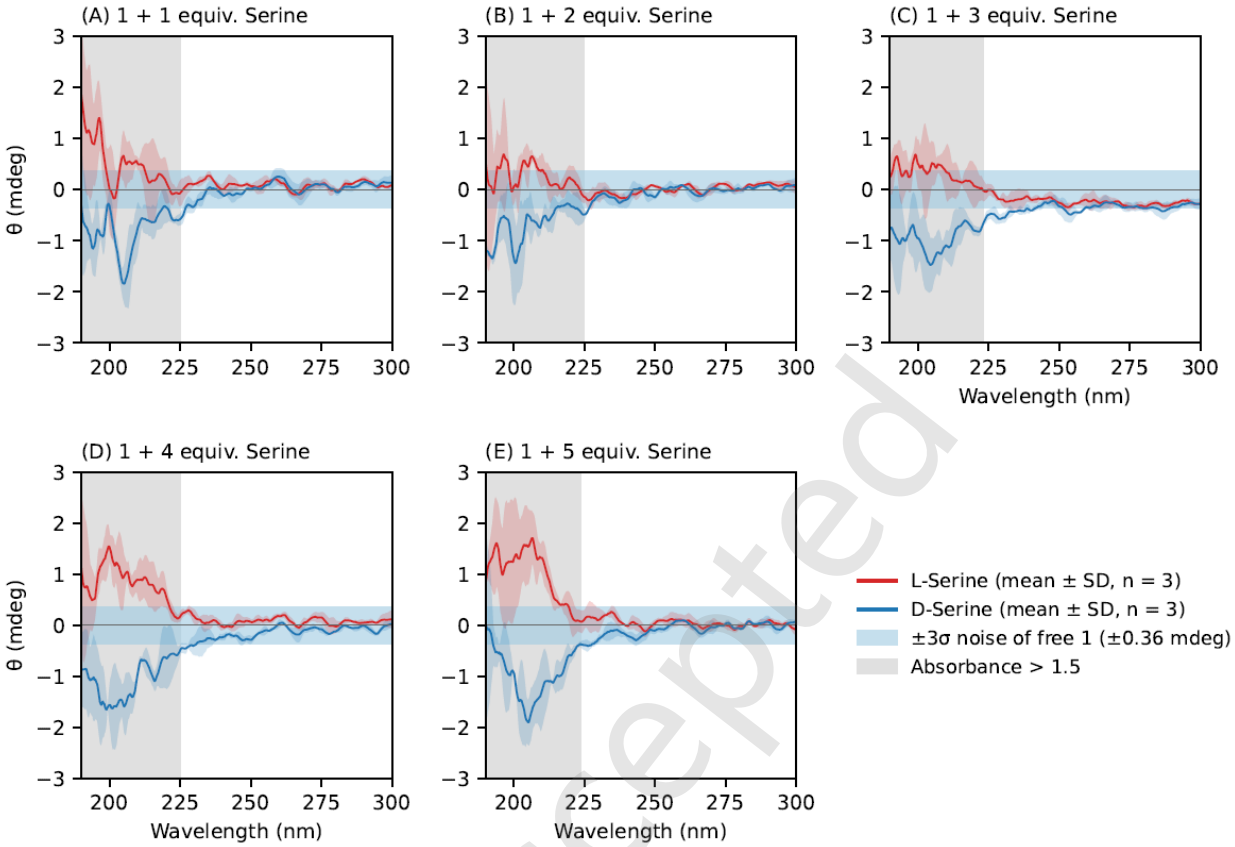

Fig. S9
CD spectra of {α_2-P_2W_{17}} **1 (pH** 3.5, 25 °C) with (A–E) 1–5 equivalents of L-Serine (red) or D-Serine (blue); lines are means of three scans and shaded bands ±1 SD. Blue band: ±3σ noise of free 1 (±0.36 mdeg); grey region: absorbance > 1.5.

Just Accepted

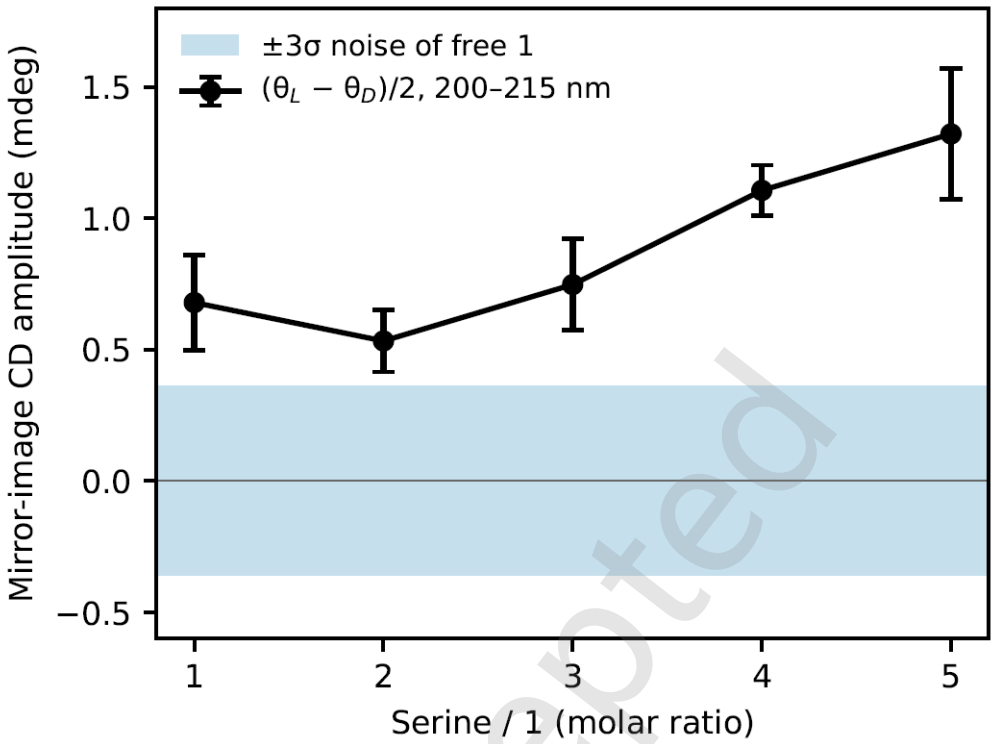

Fig. S10

Mirror-image CD amplitude (θL − θD)/2, averaged over 200–215 nm, of {α_2-P_2W_{17}} with 1–5 equivalents of L- or D-Serine (mean ± SD over all L/D scan combinations). Blue band: ±3σ noise of free {α_2-P_2W_{17}}. The amplitude exceeds the noise at all ratios and increases with Serine content; because this region overlaps the intrinsic CD band of Serine, it includes a contribution from the free amino acid.

Just Accepted

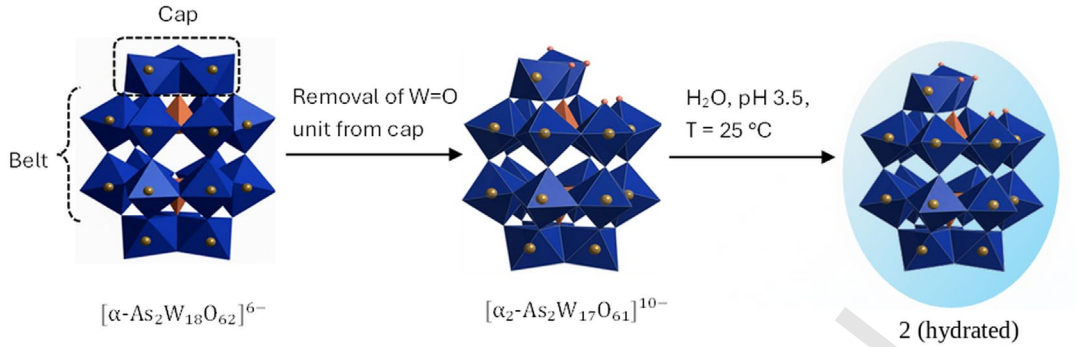

Fig. S11
The monolacunary α_2-Dawson ion is formed by removing a W=O group from one of the two caps of $\{\alpha\text{-As}_2W_{18}\}$ to form the $\{\alpha_2\text{-As}_2W_{17}\}$ polyanion 2. Color code: WO_6 dark blue octahedra (W atoms, gold spheres), AsO_4 orange tetrahedra, terminal O atoms at the vacancy, small orange spheres. Light blue oval refers to the hydration shell.

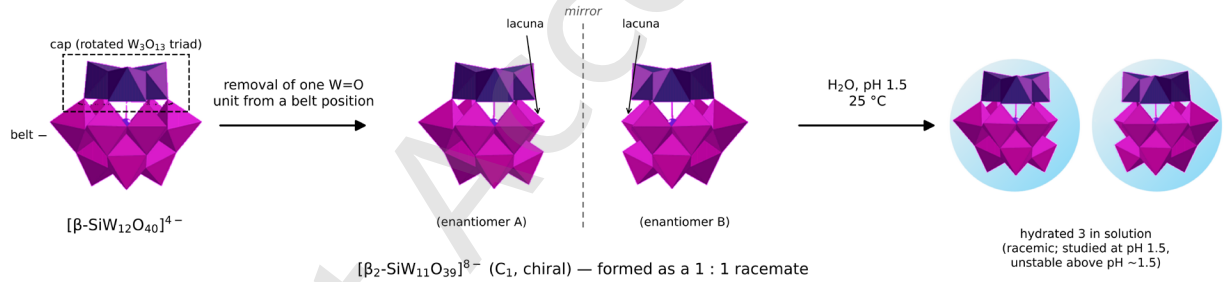

Fig. S12
Formation of the monolacunary β_2-Keggin polyanion $[\beta_2\text{-SiW}_{11}O_{39}]^{8-}$ (3) by removal of one W=O unit from a belt position of $[\beta\text{-SiW}_{12}O_{40}]^{4-}$. Because **3** has C_1 symmetry it is chiral; K-3 is obtained as a racemic (1:1) mixture of the two enantiomers A and B. Light blue ovals represents the hydration shell in water (pH 1.5, 25 °C). Color code: cap WO_6 octahedra, dark purple; belt WO_6 octahedra, pink; SiO_4, lavender.

Just Accepted

Table S1.
Amino acids used as titrants in ITC Experiments: K&D Scale and Potential Charges in H_2O with pH 3.5

Amino Acid Name	K&D Scale	Type	Isoelectric Point (pI)	Net Charge at pH = 3.5
Methionine	+1.9	Hydrophobic	~5.7	0
Alanine	+1.8		~6.0	0
Threonine	-0.7	Neutral	~5.6	0
Serine	-0.8		~5.7	0
Tryptophan	-0.9		~5.9	0
Tyrosine	-1.3		~5.7	0
Proline	-1.6		~6.3	0
Histidine	-3.2	Hydrophilic	~7.6	+1
Lysine	-3.9		~9.7	+1
Arginine	-4.0		~10.8	+1

Table S2.
Summary of the Binding and Thermodynamic Parameters during Titration of Amino Acids onto {α2-P_2W_{17}} Polyanion Obtained by ITC and AUC Experiments at Different Temperatures. Favored enantiomer: a pair is classified as discriminating when ITC (n differing by >30% or K_a by >50%) and SV-AUC ($\Delta s \geq 0.10$ S or $\Delta R_h \geq 0.05$ nm) both show a difference beyond experimental uncertainty; otherwise "None". N/A: binding heat too small to be fitted, so n, K_a, ΔH and ΔS could not be determined; ≈: approximate value from a weak fit; n ≤ 0.3 indicates negligible binding of that enantiomer.

Serine

Temp. (°C)	Favored Enantiomer	n		$K_a(M^{-1})$		ΔH (kJ/mol)		ΔS (J/mol. K)		s ± 0.05 (S)		R_h ± 0.05 (nm)	
		L-	D-	L-	D-	L-	D-	L-	D-	L-	D-	L-	D-
10	D	3.8	7.2	1.2×10	2.3×10	19.3	6.10	88.3	47.5	2.91	2.91	0.81	0.95
15	None	6.1	6.2	4.7×10^2	5.7×10^2	1.29	1.14	55.6	56.7	3.64	3.64	0.73	0.76
20	L	7.8	2.5	1.1×10^2	0.9×10	2.12	19.18	48.2	82.9	3.71	3.64	0.88	0.79
25	L	9.1	1.3	1.2×10^2	0.4×10	2.05	21.84	46.4	86.3	3.79	3.64	0.99	0.87
35	None	4.4	4.3	5.3×10^3	6.1×10^2	0.35	0.94	72.4	56.4	4.92	4.92	0.86	0.85

Threonine

Temp. (°C)	Favored Enantiomer	n		$K_a(M^{-1})$		ΔH (kJ/mol)		ΔS (J/mol. K)		s ± 0.05 (S)		R_h ± 0.05 (nm)	
		L-	D-	L-	D-	L-	D-	L-	D-	L-	D-	L-	D-
10	D	0.2	5.9	1.4×10^1	8.5×10^2	2.84	0.33	27.9	57.3	2.57	2.89	0.81	0.93
15	D	1.0	8.0	1.1×10^1	1.3×10^1	25.31	20.12	149.0	89.0	3.33	3.33	0.74	0.88
20	L	5.8	3.2	3.8×10^3	4.4×10^3	7.6	12.8	66.0	112.7	3.60	3.76	0.88	0.79
25	L	6.6	3.7	5.0×10^3	5.8×10^3	7.48	8.12	68.7	98.9	3.63	3.79	0.97	0.94
35	None	1.3	2.0	1.6×10^1	1.0×10^1	2.91	2.30	26.4	50.0	4.76	4.76	0.83	0.84

Proline

Just Accepted

Temp. (°C)	Favored Enantiomer	n		$K_a(M^{-1})$		ΔH (kJ/mol)		ΔS (J/mol. K)		s ± 0.05 (S)		R_h ± 0.05 (nm)	
		L-	D-	L-	D-	L-	D-	L-	D-	L-	D-	L-	D-
10	D	≈ 1.0	8.2	8.0×10	3.6×10	-24.7	-0.74	-50.8	27.2	2.68	2.36	0.80	1.05
15	None	≈ 0.0	≈ 0.0	N/A	N/A	N/A	N/A	N/A	N/A	3.23	3.23	0.80	0.80
20	None	N/A	N/A	N/A	N/A	N/A	N/A	N/A	N/A	3.30	3.30	0.82	0.82
25	None	N/A	N/A	N/A	N/A	N/A	N/A	N/A	N/A	3.37	3.37	0.91	0.91
35	L	3.5	1.7	9.9×10	7.3×10	5.12	6.68	54.4	51.9	4.65	4.95	0.89	0.80

Tyrosine

Temp. (°C)	Favored Enantiomer	n		$K_a(M^{-1})$		ΔH (kJ/mol)		ΔS (J/mol. K)		s ± 0.05 (S)		R_h ± 0.05 (nm)	
		L-	D-	L-	D-	L-	D-	L-	D-	L-	D-	L-	D-
10	D	≈ 1.0	8.6	N/A	3.9×10	N/A	-166	N/A	-555.0	2.65	3.37	0.82	0.85
15	None	≈ 0.0	≈ 0.0	N/A	N/A	N/A	N/A	N/A	N/A	3.18	3.18	0.75	0.75
20	None	N/A	N/A	N/A	N/A	N/A	N/A	N/A	N/A	3.34	3.34	0.81	0.81
25	None	N/A	N/A	N/A	N/A	N/A	N/A	N/A	N/A	3.37	3.37	0.91	0.91
35	None	2.3	1.9	8.9×10	7.3×10	3.06	1.30	104.7	173.9	4.64	4.64	0.90	0.88

Alanine

Temp. (°C)	Favored Enantiomer	n		$K_a(M^{-1})$		ΔH (kJ/mol)		ΔS (J/mol. K)		s ± 0.05 (S)		R_h ± 0.05 (nm)	
		L-	D-	L-	D-	L-	D-	L-	D-	L-	D-	L-	D-
10	D	3.3	10.1	1.3×10	1.0×10	2.37	0.88	27.4	16.2	2.78	2.53	0.80	1.00
15	D	≈ 1.0	4.2	1.1×10	6.2×10^3	0.39	0.31	20.5	73.7	3.33	3.18	0.73	0.82
20	None	≈ 1.0	≈ 1.0	8.9×10^3	9.5×10^3	2.12	2.35	81.8	84.1	3.38	3.38	0.82	0.82
25	None	1.1	0.9	8.7×10^3	9.7×10^3	2.04	2.66	81.2	85.3	3.64	3.64	0.86	0.86
35	None	3.5	3.9	4.5×10^2	5.8×10^2	0.86	0.92	81.3	60.3	5.25	5.25	0.85	0.85

Methionine

Temp. (°C)	Favored Enantiomer	n		$K_a(M^{-1})$		ΔH (kJ/mol)		ΔS (J/mol. K)		s ± 0.05 (S)		R_h ± 0.05 (nm)	
		L-	D-	L-	D-	L-	D-	L-	D-	L-	D-	L-	D-
10	D	≈ 1.0	8.3	N/A	1.1×10	N/A	16.4	N/A	77.1	2.68	3.32	0.80	0.81
15	D	3.2	6.1	1.1×10	1.5×10	-1.81	-1.85	12.9	12.7	3.33	3.03	0.80	0.96
20	None	1.6	1.4	8.8×10^2	9.4×10	0.72	0.60	56.6	39.8	3.38	3.38	0.80	0.78
25	None	1.9	1.2	8.7×10^2	9.0×10^2	0.81	0.53	59.0	36.7	3.64	3.64	0.90	0.88
35	None	2.5	2.8	5.3×10^2	6.1×10^2	0.99	1.13	66.3	82.3	6.04	6.04	0.75	0.69

Tryptophan

Temp. (°C)	Favored Enantiomer	n		$K_a(M^{-1})$		ΔH (kJ/mol)		ΔS (J/mol. K)		s ± 0.05 (S)		R_h ± 0.05 (nm)	
		L-	D-	L-	D-	L-	D-	L-	D-	L-	D-	L-	D-
10	D	5.3	9.9	7.3×10^2	2.4×10^2	0.28	0.90	94.1	48.8	2.91	2.53	0.90	1.22
15	D	6.1	8.2	6.1×10^2	3.2×10^2	0.40	0.86	89.2	52.9	3.31	3.31	0.94	1.01
20	L	7.6	N/A	2.1×10^2	1.7×10^2	-0.50	N/A	52.2	N/A	3.38	3.51	1.10	0.77
25	L	8.5	N/A	1.5×10^2	N/A	-0.70	N/A	39.0	N/A	3.48	3.64	1.09	0.84
35	None	1.8	2.0	7.2×10^2	8.1×10^2	0.63	0.88	99.3	54.4	4.44	4.44	0.93	0.94

Histidine

Temp. (°C)	Favored Enantiomer	n		$K_a(M^{-1})$		ΔH (kJ/mol)		ΔS (J/mol. K)		s ± 0.05 (S)		R_h ± 0.05 (nm)	
		L-	D-	L-	D-	L-	D-	L-	D-	L-	D-	L-	D-
10	D	3.8	9.3	1.1×10^1	1.9×10^2	-5.9	-2.4	2.36	35.3	2.91	3.10	0.82	0.90
15	None	2.2	2.3	6.5×10^2	7.8×10^2	1.8	1.6	58.0	57.0	3.33	3.33	0.78	0.78
20	None	3.1	3.0	3.0×10^3	2.1×10^3	4.9	3.9	72.2	71.3	3.48	3.48	0.87	0.87
25	None	4.3	4.4	1.5×10^4	1.7×10^4	5.73	3.4	93.7	89.1	3.67	3.67	0.97	0.97

Just Accepted

35	L	6.9	6.1	4.9×10^{3}	2.7×10^{3}	7.26	10.2	94.2	98.7	5.40	5.10	0.96	0.95

Lysine

Temp. (°C)	Favored Enantiomer	n		$K_a(M^{-1})$		ΔH (kJ/mol)		ΔS (J/mol. K)		s ± 0.05 (S)		R_h ± 0.05 (nm)	
		L-	D-	L-	D-	L-	D-	L-	D-	L-	D-	L-	D-
10	D	0.2	3.0	4.9×10^{2}	5.3×10^{2}	-8.1	-9.2	23.3	19.7	2.59	2.59	0.81	0.89
15	D	0.8	4.9	1.1×10^{2}	2.0×10^{2}	-33.7	-4.6	-77.9	28.0	3.18	3.18	0.77	0.88
20	None	2.1	2.3	5.8×10^{2}	6.2×10^{2}	-10.2	-9.6	-22.0	-21.2	3.31	3.31	0.88	0.89
25	None	3.0	3.5	6.4×10^{2}	5.6×10^{2}	-7.0	-7.7	-15.5	-15.2	3.38	3.38	1.00	1.02
35	L	5.8	5.1	4.1×10^{3}	1.0×10^{3}	-0.8	-1.2	66.4	53.6	4.65	4.95	0.98	0.90

Arginine

Temp. (°C)	Favored Enantiomer	n		$K_a(M^{-1})$		ΔH (kJ/mol)		ΔS (J/mol. K)		s ± 0.05 (S)		R_h ± 0.05 (nm)	
		L-	D-	L-	D-	L-	D-	L-	D-	L-	D-	L-	D-
10	D	2.1	9.2	4.0×10	3.1×10^{2}	-23.8	-1.3	-53.2	43.1	2.58	2.73	0.88	1.08
15	D	4.9	7.5	1.5×10^{2}	2.5×10^{2}	-10.6	-7.4	4.5	20.3	3.18	3.18	0.91	0.99
20	None	3.6	3.4	3.2×10^{2}	3.5×10^{2}	-10.7	-11.1	8.9	6.1	3.31	3.31	0.94	0.94
25	None	3.2	2.5	3.5×10^{2}	4.1×10^{2}	-10.6	-11.6	13.1	-12.8	3.38	3.38	1.03	1.00
35	L	4.4	0.9	1.1×10^{3}	6.0×10^{2}	-3.9	-20.5	45.9	-13.3	5.40	5.10	0.83	0.77

Table S3.

Summary of the Binding and Thermodynamic Parameters during Titration of Amino Acids onto {α2-As2W17} Polyanion Obtained by ITC and AUC Experiments at Different Temperatures. Favored enantiomer: a pair is classified as discriminating when ITC (n differing by >30% or K_a by >50%) and SV-AUC ($\Delta s \geq 0.10$ S or $\Delta R_h \geq 0.05$ nm) both show a difference beyond experimental uncertainty; otherwise "None". N/A: binding heat too small to be fitted, so n, K_a, ΔH and ΔS could not be determined; ≈: approximate value from a weak fit; n ≤ 0.3 indicates negligible binding of that enantiomer.

Serine

Temp. (°C)	Favored Enantiomer	n		$K_a(M^{-1})$		ΔH (kJ/mol)		ΔS (J/mol. K)		s ± 0.05 (S)		R_h ± 0.05 (nm)	
		L-	D-	L-	D-	L-	D-	L-	D-	L-	D-	L-	D-
10	None	0.1	0.3	2.4×10	1.4×10	4.33	3.18	40.6	32.5	3.23	3.23	0.72	0.73
25	L	4.7	3.9	2.4×10^{2}	1.5×10^{2}	1.93	2.28	52.0	49.5	4.84	4.64	0.72	0.74
35	L	9.2	3.2	3.6×10^{1}	1.5×10	0.99	2.77	33.0	31.6	5.96	5.96	0.74	0.65

Threonine

Temp. (°C)	Favored Enantiomer	n		$K_a(M^{-1})$		ΔH (kJ/mol)		ΔS (J/mol. K)		s ± 0.05 (S)		R_h ± 0.05 (nm)	
		L-	D-	L-	D-	L-	D-	L-	D-	L-	D-	L-	D-
10	D	1.3	5.8	2.2×10^{2}	2.0×10^{2}	5.14	0.11	62.5	60.6	3.33	3.18	0.70	0.82
25	L	7.3	3.9	5.0×10^{2}	1.5×10^{2}	0.41	2.28	53.0	49.6	4.64	4.75	0.81	0.73
35	L	5.3	0.1	3.8×10	2.6×10	0.58	3.17	32.1	36.8	5.15	5.15	0.73	0.64

Proline

Temp. (°C)	Favored Enantiomer	n		$K_a(M^{-1})$		ΔH (kJ/mol)		ΔS (J/mol. K)		s ± 0.05 (S)		R_h ± 0.05 (nm)	
		L-	D-	L-	D-	L-	D-	L-	D-	L-	D-	L-	D-
10	None	9.1	9.4	1.3×10	1.2×10	-3.12	-3.05	9.2	8.4	2.93	2.93	0.96	0.97
25	None	10.0	10.0	1.0×10	1.0×10	-2.37	-1.96	11.2	12.6	4.24	4.24	0.94	0.94
35	None	10.0	10.0	3.8×10	4.0×10	-0.74	-1.96	27.8	12.8	5.15	5.15	0.81	0.81

Alanine

Just Accepted

Temp. (°C)	Favored Enantiomer	n		$K_a(M^{-1})$		ΔH (kJ/mol)		ΔS (J/mol. K)		s ± 0.05 (S)		R_h ± 0.05 (nm)	
		L-	D-	L-	D-	L-	D-	L-	D-	L-	D-	L-	D-
10	D	2.8	6.0	1.8×10	1.1×10	-5.00	-1.17	15.0	12.3	2.73	3.03	0.87	0.84
25	L	9.9	0.3	5.1×10^2	2.5×10^2	-6.36	-5.77	31.5	26.7	4.14	4.44	0.91	0.71
35	L	6.1	3.9	1.5×10^3	3.8×10^2	-0.15	-0.23	60.4	48.5	5.05	5.45	0.73	0.65

Methionine

Temp. (°C)	Favored Enantiomer	n		$K_a(M^{-1})$		ΔH (kJ/mol)		ΔS (J/mol. K)		s ± 0.05 (S)		R_h ± 0.05 (nm)	
		L-	D-	L-	D-	L-	D-	L-	D-	L-	D-	L-	D-
10	D	3.8	9.3	1.1×10	1.9×10^2	-0.98	-2.35	16.4	35.3	3.33	3.23	0.77	0.93
25	L	9.8	6.3	2.9×10	1.6×10	-1.14	-3.15	24.1	13.0	4.00	4.35	1.05	0.88
35	L	3.5	1.4	1.4×10	1.1×10	2.19	2.98	28.4	26.4	5.15	5.00	0.65	0.56

Histidine

Temp. (°C)	Favored Enantiomer	n		$K_a(M^{-1})$		ΔH (kJ/mol)		ΔS (J/mol. K)		s ± 0.05 (S)		R_h ± 0.05 (nm)	
		L-	D-	L-	D-	L-	D-	L-	D-	L-	D-	L-	D-
10	None	4.5	4.9	1.67×10^2	1.68×10^2	-7.75	-6.82	15.2	18.5	2.93	2.93	0.90	0.91
25	None	7.5	7.6	8.50×10	8.50×10	-3.10	-3.02	26.6	26.8	4.34	4.34	0.85	0.83
35	None	9.7	9.2	6.04×10	5.97×10	0.13	-0.62	34.5	32.0	5.25	5.25	0.85	0.83

Lysine

Temp. (°C)	Favored Enantiomer	n		$K_a(M^{-1})$		ΔH (kJ/mol)		ΔS (J/mol. K)		s ± 0.05 (S)		R_h ± 0.05 (nm)	
		L-	D-	L-	D-	L-	D-	L-	D-	L-	D-	L-	D-
10	None	5.8	5.2	5.20×10^2	5.31×10^2	-4.88	-4.91	35.5	34.8	3.03	3.03	0.89	0.88
25	None	8.1	7.9	4.80×10^2	4.66×10^2	-4.87	-4.62	35.0	35.5	4.14	4.14	0.97	0.96
35	None	5.0	4.8	4.51×10^2	4.38×10^2	-4.84	-3.91	35.1	40.0	5.15	5.15	0.74	0.74

Arginine

Temp. (°C)	Favored Enantiomer	n		$K_a(M^{-1})$		ΔH (kJ/mol)		ΔS (J/mol. K)		s ± 0.05 (S)		R_h ± 0.05 (nm)	
		L-	D-	L-	D-	L-	D-	L-	D-	L-	D-	L-	D-
10	None	8.3	8.9	5.3×10^2	5.2×10^2	-3.83	-3.87	38.5	38.7	2.83	2.83	1.07	1.09
25	None	5.3	4.8	5.0×10^2	4.8×10^2	-3.76	-3.80	38.8	38.6	4.24	4.24	0.90	0.88
35	None	4.5	4.9	4.7×10^2	4.6×10^2	-3.78	-3.74	38.9	38.7	5.25	5.25	0.74	0.75

Just Accepted